UNIVERSITY OF CALIFORNIA
Santa Barbara

Estimates of Hydrologic Properties in Upper Ocean Crust of Juan de Fuca Ridge Eastern Flank Using Sulfur Hexafluoride Gas Tracer in Cross-Hole Multi-Scale Injection Experiment

A Thesis submitted in partial satisfaction of the
requirements for the degree Master of Science
in Geological Sciences

by

Nicole Margoritte Neira

Committee in charge:

Professor Jordan F. Clark, Chair

Professor Rachel M. Haymon

Professor Syee Weldeab

December 2014

The thesis of Nicole Margoritte Neira is approved.

_____

Rachel M. Haymon

_____

Syee Weldeab

_____

Jordan F. Clark, Committee Chair

December 2014

Estimates of Hydrologic Properties in Upper Ocean Crust of Juan de Fuca Ridge Eastern Flank Using Sulfur Hexafluoride Gas Tracer in Cross-Hole Multi-Scale Injection Experiment

by

Nicole Margoritte Neira

ACKNOWLEDGEMENTS

Funding was provided by NSF grant OCE-1031352 and OCE-1260353. This work would not be possible without the hard work of the *ROV Jason* pilot crew and the *R/V Atlantis* personnel. I would like to acknowledge Dr. Rachel Haymon for her expertise in mid-ocean ridge hydrothermal systems. Her personal efforts and investment into understanding the project's implications on my behalf was beyond my expectations. Her persistence and genuine scientific curiosity make her a brilliant scientist and mentor. I would also like to dedicate this Thesis to my family for their support: Mauricio, Mom, Dad, Ale, Claudio, and Michael.

ABSTRACT

Estimates of Hydrologic Properties in Upper Ocean Crust of Juan de Fuca Ridge Eastern Flank Using Sulfur Hexafluoride Gas Tracer in Cross-Hole Multi-Scale Injection Experiment

by

Nicole Margoritte Neira

A tracer injection experiment was performed in 3.5 Myr old seafloor comprised of sediment-buried abyssal hills oriented N20°E, and located 100 km east of the Endeavor Segment of the Juan de Fuca spreading ridge in the northeastern Pacific. In the summer of 2010, a mixture of tracers (metal salts, dissolved sulfur hexafluoride [SF_6], microspheres) was injected into the crust via borehole 1362B as part of a 24-hour injection experiment during IODP Expedition 327. Fluid samples were subsequently collected from 1362B, and from four additional holes (1026B, 1362A, 1301A, and 1301B) located 300 to 550 m away from the injection hole. The borehole array penetrates a hydrothermal fluid flow system thought to be flowing from SW to NE along a buried abyssal hill often referred to as Second Ridge (SR). Hydrothermal flow is thought to be controlled by a series of exposed volcanic

outcrops located along the same buried hill. According to the hypothesis, recharge of bottom seawater occurs through Grizzly Bare, an exposed outcrop 52 km south of the borehole array, and discharge seeps through Baby Bare and possibly also Mama Bare outcrops, which are both located within 5 km to the existing boreholes. The goal of this study is to test hypothesized fluid flow direction, flow velocity and crustal permeability using the conservative gas tracer SF_6.

Two small cylinders of SF_6 were injected at a fluid pumping rate of 6.7 L/s for 20.2 hours, resulting in a mean concentration of 47.6 μM or 47,600 nM (total of ~23 mol of SF_6 was injected). Borehole fluid was continuously sampled in 1.8 mm ID copper tubes using osmosamplers (OS) from each of the long-term, subseafloor observatories (known as CORKs) that had previously been installed in the boreholes. The OS spools were recovered using the *ROV Jason* in 2011 and 2013. Following recovery, fluid samples were transferred into evacuated vials for measuring SF_6 via gas chromatography in a shore-based laboratory. Results of samplers recovered in 2011 indicate the first arrival of injected SF_6 ~305 days after injection at Hole 1301A, located 550 m south of the injection Hole 1362B. This suggests that the mean lateral transport of tracer is ~1.8 m/day (660 m/yr), a rate at the upper end of previous upper crustal fluid flow velocity estimates.

The first detection of an SF_6 patch south of the injection source apparently contradicts the prior hypothesis that crustal fluid is flowing northward from Grizzly Bare to Baby and Mama Bares, but there are extensive leaks in Hole 1301A, which may have inadvertently pulled SF_6 southwards. CORKs 1301B and 1026B are also

leaking hydrothermal fluid, and any data collected from these holes should be interpreted carefully. Both 1362A and injection Hole 1362B are operating as intended with no known leaks, although a discharge valve was opened at 1362B in 2011 and closed in 2013. Following this perturbation to the flow field, the 1362A valve was opened in 2013 and then closed in 2014. Tracer was detected in both 1362A and 1362B from the beginning of sampling in 2013, one year after injection. The mean tracer concentration for Holes 1362B and 1362A was 4.6 nM and 4.5 nM, respectively. The sustained signal at these CORKs suggests a hovering of an SF_6 patch spanning at least 311 meters in the region. The detection of a considerable amount of tracer to the north at 1362A is consistent with the hypothesized SW-NE fluid flow direction. The hydrogeological fabric at our site appears to be heterogeneous, with fluid transport occurring through small, isolated permeable zones found in the upper volcanic portion of the ocean crust.

TABLE OF CONTENTS

LIST OF FIGURES

I. INTRODUCTION

Hydrothermal fluid flow within the mid-ocean ridge is known to be a wide-spread natural phenomenon. Cold, bottom seawater enters the ocean crust through cracks and fractures [*Macdonald*, 2001*; Davis et al.*, 2001] and is heated, thereby cooling the crust [*Stein and Stein*, 1994]. At recharge zones, seawater entering the crust (**Figure 1A**) undergoes oxidation, alkali fixation and metal extraction as it interacts with basalt and warms. The resultant hydrothermal water is chemically distinct from seawater and discharges into the ocean in focused areas, as seen at mid-ocean ridge hydrothermal vents [*Wheat and Mottl*, 2000; *Alt and Teagle*, 2003]. It is estimated that the total seawater volume flows through the upper ocean crust in approximately 200,000 years [*Johnson and Prius*, 2003], causing massive thermal, chemical and biological exchanges between the oceans and the solid earth, and hydration of ocean lithosphere. Subduction of hydrated lithosphere plays a role in melting mantle wedges in subduction zones [*Till et al*., 2012], arc volcanism and mantle heterogeneities [*Zindler and Jagoutz*, 1988; *Alt*, 1995].

A. Purpose of Study

Mid-ocean ridge hydrothermal circulation is a major component in large-scale chemical and thermal exchanges and helps support biological activity on, above, and under the seafloor. Much has been learned about the transfer of heat at the ridge crest from studying hydrothermal vent systems, but scientists know much less about hydrothermal heat transfer through the vastly larger regions on ridge flanks [*Stein et*

al., 1995]. The purpose of this project, within a broader context, is to contribute to the quantification of the large-scale geochemical and heat fluxes in ridge flank settings by constraining the hydrological properties of the upper ocean crust. Yielding directly-measured values in this less-known marine environment is an important task because 30% of the Earth's surface area is comprised of abyssal hills and nearly 70% of the planet is overlain by oceanic crust [*Sverdrup et al*., 2004].

1. Hydrothermal Systems at Mid-Ocean Ridges

The occurrence of seawater continuously recycling through the ocean crust via convective hydrothermal circulation has been recognized for many years. Seismic refraction studies from the 1960s reveal a vertically structured igneous stratigraphy created by magma injection and eruption along and near spreading ridges, where plates of lithosphere are splitting and moving apart [*Solomon and Toomey*, 1992]. As new igneous seafloor migrates via seafloor spreading onto the ridge flank, it continues to cool via heat conduction and hydrothermal heat loss. One of the seismic observations is an increase in seismic wave velocities in ocean crust from spreading axis to ridge flank over a distance of hundreds of kilometers (**Figure 1B**) [*Stein et al.*, 1995, seismic studies references therein]. This is inferred to be a consequence of decreasing crustal porosity as the crust ages and spreads away from the ridge axis onto the ridge flanks [*Carbotte*, 2001; *Newman et al*., 2011]. The inferred porosity reduction is attributed to hydrothermal alteration that results in precipitation of secondary minerals and filling of void space. Petrographic analyses of ridge-flank crust core samples and ophiolites reveal mineral assemblages and veins that are

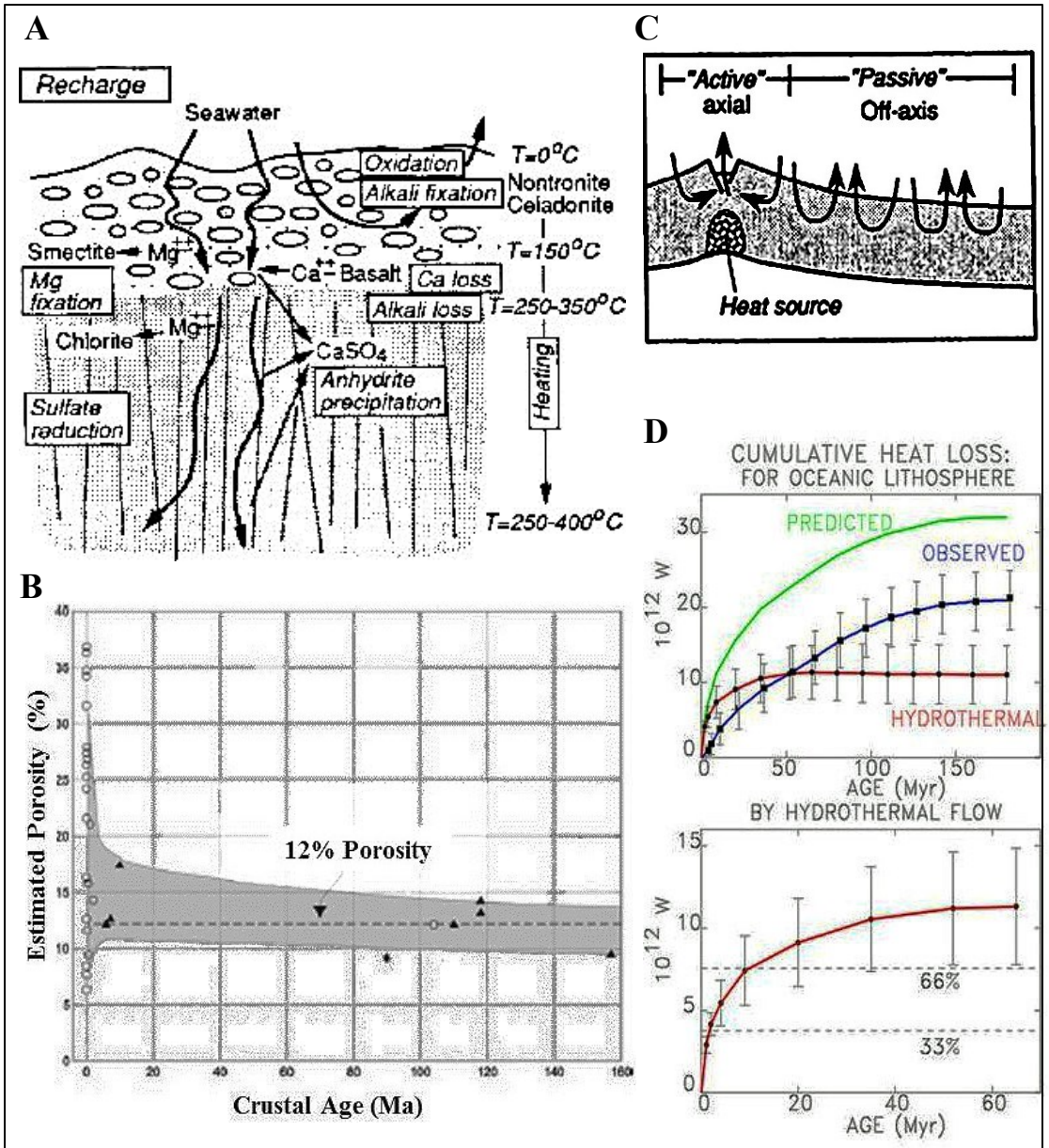

FIGURE 1. [A] Cross-sectional diagram of geochemical cycle at a recharge site in the upper ocean crust. Cold bottom seawater penetrates through warmer rock basement causing a massive ion-exchange between fluid and volcanics [from *Alt*, 1995]. **[B]** Crustal porosity as a function of age [from *Johnson and Pruis*, 2003]. **[C]** Flow regimes characterized by location relative to mid-ocean ridge axis. Active circulation occurs above fixed heat sources below axis. Passive circulation results from residual heat (lithospheric cooling) within ridge flanks [from *Alt*, 1995]. **[D]** (Green) Heat flow vs. age predicted for a conductively cooled ocean lithospheric plate; (Blue) Observed heat flow vs. age is less than predicted due to convective heat loss (Red) [from *Stein et al.*, 1995].

formed only through the presence of vigorous high-temperature fluid convection through the crust [*Staudigel et al*., 1981; *Nehlig and Juteau*, 1988; *Von Damm*, 1995; *Bach et al*., 2001; *Alt and Teagle*, 2003; *Benjamin and Haymon*, 2006].

Observations made on the fast-spreading East Pacific Rise (EPR) led to the conclusion that magma is the principal driving force for ridge crest hydrothermal systems at full spreading rates >4cm/yr [*Haymon et al*., 1991; *Haymon*, 1996; *Von Damm*, 2004]. Subsequently, *Carbotte et al*. [2012] used seismic velocity surveys to confirm the presence of an axial magma chamber (AMC) beneath major vent fields at the Endeavour segment on the Juan de Fuca (JdF) ridge crest, 100 km directly west of our study site. Magma at a ridge crest can erupt through the sheeted dike complex and interact simultaneously with seawater residing in the fracture system above. This "active" hydrothermal circulation can still occur in spreading centers with a lower magma supply; instead, it is the recharging seawater itself that penetrates the freezing magma chamber via fracture permeability [*Lister*, 1972; *Haymon*, 1996].

In contrast, ridge-flank hydrothermal systems are considered "passive" and are mostly driven by residual heat in the lithosphere (**Figure 1C**), which is a much larger and spatially pervasive source of heat than ridge-axis magma chambers [*Stein et al.*, 1995; *Alt*, 1995]. In a passive fluid flow system, low-temperature (<200°C) flow often occurs along-strike (i.e., parallel to the ridge axis; [*Haymon*, 1996]) along normal faults characteristic of mid-ocean ridge extension [*Macdonald*, 2001], and/or through seamounts exposed directly to the bottom ocean [*Davis*, 1980]. The presence of a thick sediment deposit, an essentially impermeable layer, can influence the

regional heat flow by increasing the thermal gradient [*Lister*, 1972].

Ridge flank circulation is a mechanism for large-magnitude heat loss in the ocean crust [*Mottl and Wheat*, 1994]. The most compelling piece of evidence for this is the large deficiency between predicted conductive heat flow and observed crustal heat flow. If heat loss occurred exclusively through conductive lithospheric cooling, observations should match heat flow predicted by the conduction-based heat loss model (**Figure 1D**). Observed heat flow values, however, are anomalously low, and this suggests significant additional heat loss via convective hydrothermal circulation through young permeable ocean crust. Heat flow measurements show most of the convective heat loss is from crust <65 Ma with 30% of the net convective hydrothermal heat flux lost from 0- 1 Ma crust and 70% lost from 1-65 Ma crust [*Stein et al.*, 1995]. *Johnson and Pruis* [2003] estimate that nearly half of all oceanic hydrothermal heat loss occurs within 5 Ma crust (**Figure 2A**). The tracer injection experiment was carried out in ~3.5 Ma crust, within the range where young, more permeable crust facilitates the largest amount of heat transport out of the upper ocean crust via hydrothermal fluid flow.

2. Previous Hydrological Estimates

Several studies have attempted to constrain the hydrological properties of the upper oceanic crust on the JdF Ridge eastern flank. One such parameter, fluid flow velocity, has been indirectly estimated using dissolved ion species and radiocarbon dating of crustal fluid sampled from boreholes on the JdF Ridge eastern flank [*Elderfield et al.*, 1999; *Wheat et al.*, 2003; *Walker et al.*, 2008]. Fluid flow velocity,

or lateral flow rate, is important to know because geochemical and nutrient cycling can be constrained from the timescales estimated. Within the JdF Ridge eastern flank, a lateral flow rate of 1-4 m/yr was estimated using the change in concentration gradients of [SO_4^{2-}] and [Cl^-] in fluid sampled just below the sediment-volcanic basement interface [*Elderfield et al.*, 1999]. Another study by *Wheat et al*. [2000] used diffusive ion-exchange rates to calculate a lateral flow rate of 80 m/yr (assuming an effective porosity of 0.1).

The radiocarbon dating method calculates flow rate with a simple piston flow model (i.e. velocity = distance between two fluid sampling points divided by radiocarbon age difference). There are several different estimates presented. The *Elderfield et al.* [1999] study calculated a lateral flow rate of 1-3 m/yr, whereas *Walker et al*. [2008] yielded a flow rate of 5.7 m/yr. *Walker et al*. [2008]'s estimate is more relevant as all fluid sampling occurred at the site of the boreholes in our study. However, the radiocarbon dating method overestimates ages and underestimates velocities when molecular diffusion is an important mode of transport [*Stein and Fisher*, 2003]. Molecular diffusion will have the greatest effect in fluid transport (relative to advection and dispersion) when most of the rock matrix is comprised of thick aquitards that leak older fluid into thin permeable zones with younger fluid [*Sanford*, 1997]. Mixing of these waters will increase the diffusion correction ratio (pore space of aquitard to aquifer) and in turn yield a much larger velocity (see Eq.1, modified from *Bethke and Johnson*, 2002). As a result, radiometric estimates are on the lower end of potential flow rates in the area. A volcanic rock matrix, such as at

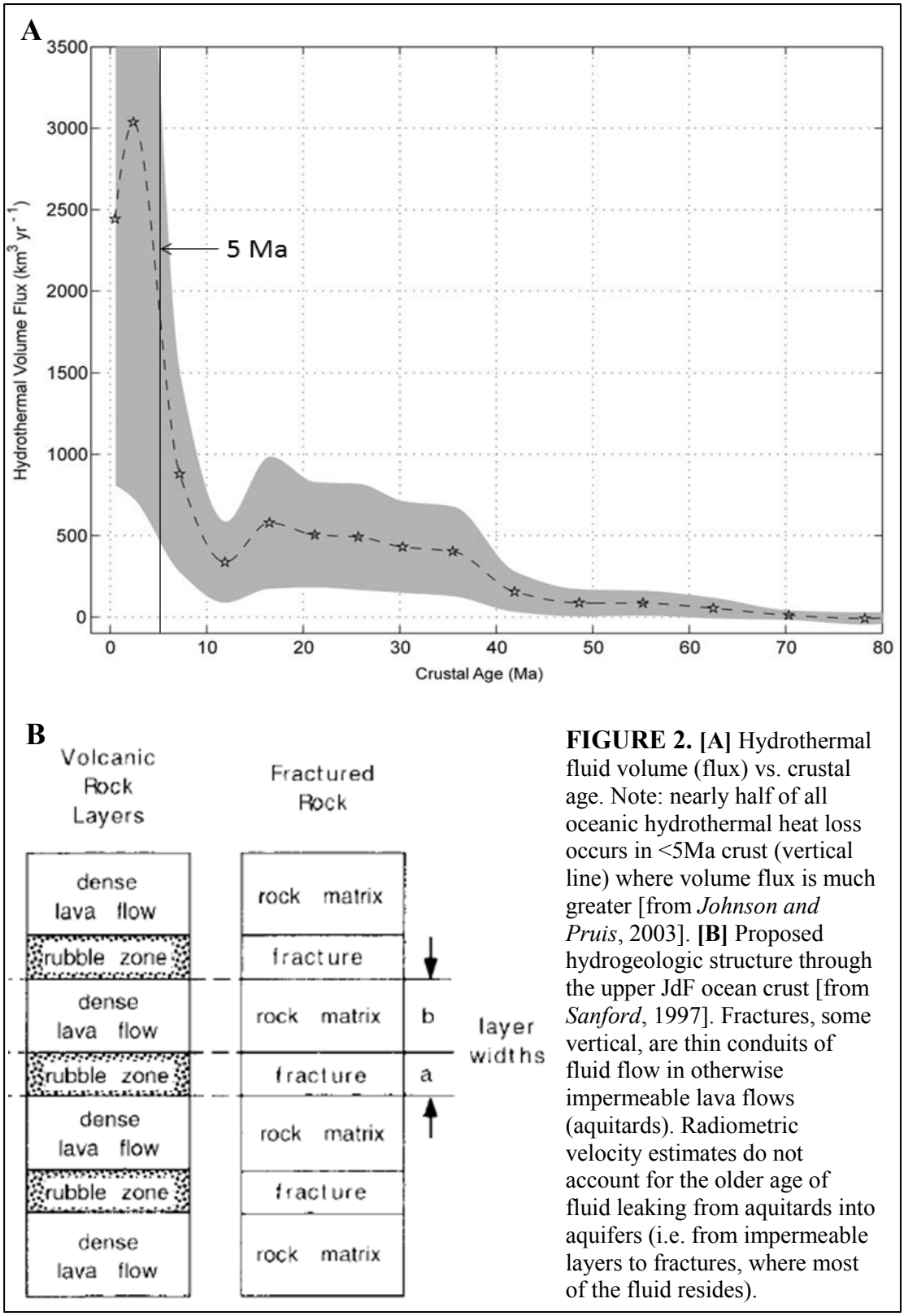

FIGURE 2. [A] Hydrothermal fluid volume (flux) vs. crustal age. Note: nearly half of all oceanic hydrothermal heat loss occurs in <5Ma crust (vertical line) where volume flux is much greater [from *Johnson and Pruis*, 2003]. **[B]** Proposed hydrogeologic structure through the upper JdF ocean crust [from *Sanford*, 1997]. Fractures, some vertical, are thin conduits of fluid flow in otherwise impermeable lava flows (aquitards). Radiometric velocity estimates do not account for the older age of fluid leaking from aquitards into aquifers (i.e. from impermeable layers to fractures, where most of the fluid resides).

the JdF Ridge eastern flank, will have thin aquifers in the form of fractures, and thicker aquitards in the form of un-cracked, low-porosity massive lava flows (**Figure 2B**). It is crucial for ridge flank fluid systems to take into account the mass exchange from less permeable basement [*Bethke and Johnson*, 2002].

$$V_x = \frac{[1+(\eta_{aqt} \times \ell / \eta_{aqf} \times L)]}{(\Delta t / \Delta x)} \quad \text{(Eq.1)}$$

where: V_x is flow velocity, η_{aqt} and η_{aqf} are, respectively, the porosity in aquitard and aquifer; ℓ and L are, respectively, the aquitard and aquifer thicknesses; Δt is radiometric age difference; and Δx is the distance between the two sampling points.

A number of publications have focused on estimating permeability for the upper igneous crust at JdF. Permeability, or connected pore space, is an important parameter as it houses the hydrothermal aquifer and directly affects the transport of fluid, solutes, and heat [*Fisher*, 1998]. Based on hydrologic packer tests at Hole 1301 during drilling, *Becker and Fisher* [2008]'s model estimates permeability in the range of $1-3 \times 10^{-12}$ m^2. *Fisher et al*. [2008] used pressure records from Hole 1027C before and after its installation as well as 1301B's pressure response to said installation to estimate a permeability of $0.7-2 \times 10^{-12}$ m^2. *Davis et al*. [2010] took advantage of the initial leak in 1301B after installation and used a finite groundwater model to calculate a 3-5 $\times 10^{-13}$ m^2 permeability at the study site. It is clear that the difference in permeability estimates can depend on methodology and/or model assumptions used. However, hydrologic permeability anisotropy governed by fault and crack orientation remains the most likely possibility for this deviation [*Stein and Fisher*,

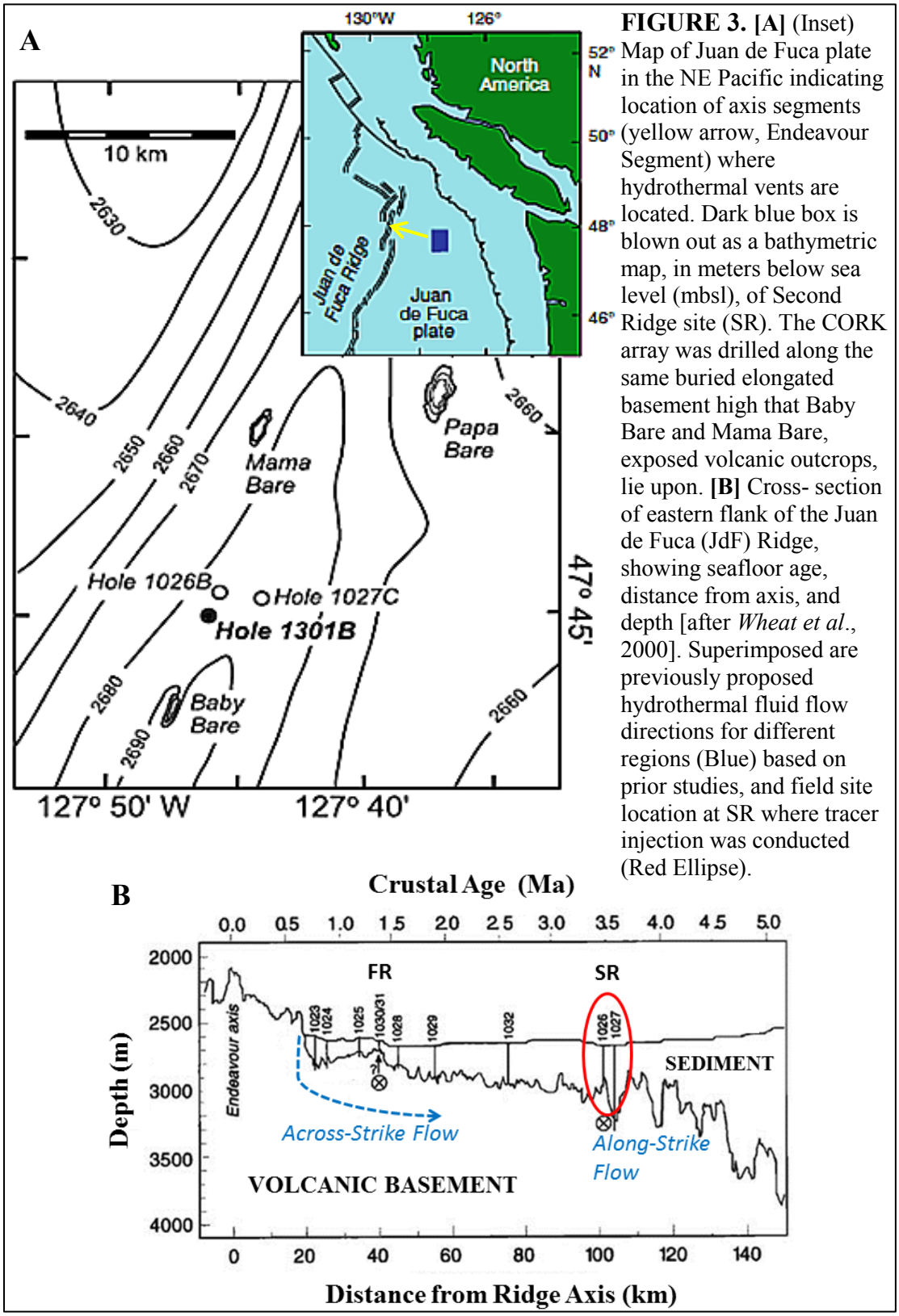

FIGURE 3. [A] (Inset) Map of Juan de Fuca plate in the NE Pacific indicating location of axis segments (yellow arrow, Endeavour Segment) where hydrothermal vents are located. Dark blue box is blown out as a bathymetric map, in meters below sea level (mbsl), of Second Ridge site (SR). The CORK array was drilled along the same buried elongated basement high that Baby Bare and Mama Bare, exposed volcanic outcrops, lie upon. **[B]** Cross- section of eastern flank of the Juan de Fuca (JdF) Ridge, showing seafloor age, distance from axis, and depth [after *Wheat et al*., 2000]. Superimposed are previously proposed hydrothermal fluid flow directions for different regions (Blue) based on prior studies, and field site location at SR where tracer injection was conducted (Red Ellipse).

2003; *Fisher et al*., 2008; *Becker and Fisher*, 2008; *Davis et al*., 2010; *Winslow et al.*, 2013]. This is why using a conservative anthropogenic tracer in the ocean crust is ideal as it can directly track fluid transport in the subseafloor and a more accurate permeability can be estimated.

B. Geological Setting

The Juan de Fuca mid-ocean ridge is an intermediate spreading center with a spreading rate of about 5.6 cm/yr [*Newman et al*., 2011]. It is composed of seven major segments and has active hydrothermal venting along its axis (**Figure 3A**). The eastern flank older than 0.9 Ma (20 km away from axis) is blanketed by an unusually thick sediment layer, ranging from 300-600 m, due to turbidite flows deposited during the Pleistocene when sea level was lower than at present [*Wheat et al.*, 2000]. It is important to note that the large amount of sediment above acts as an insulator, and, along with a vigorous convection underneath, is keeping the basement at our site at an isothermal temperature of 64°C [*Wheat and Mottl*, 2000]. It also acts as a confining layer to the underlying basement aquifer.

The tracer injection was conducted on the Second Ridge (SR) site, which is located 100 km east of the Endeavour segment ridge axis. Second Ridge is the name given to this site by *Hutnak et al*. [2006] in comparing it to First Ridge (FR), an area 60 km west of SR and 40 km east of the ridge axis (**Figure 3B**), where younger thinly-sedimented basalt permits recharge of cold bottom seawater into the volcanic upper crust. The SR site has six boreholes which are drilled and cased through the

sediment layer and into no more than 320 m of upper extrusive pillow deposits. Five of the boreholes (1026B, 1301A, 1301B, 1362A, and 1362B) were installed on a basement bathymetric high sub-parallel to the strike of the Endeavour ridge axis (i.e., on an upfaulted abyssal hill [*Macdonald et al*., 1996] draped by sediment). One borehole (1027C) was drilled 2 km east of SR on an adjacent downfaulted bathymetric low.

C. Fluid Flow Hypothesis

When exploration began along the eastern flank of the JdF ridge four decades ago, hydrothermal fluid flow was thought of as a perpendicular flow entering from the active spreading center and being carried through the flanks hundreds of km away. Over the years, this has been accepted as a generalized concept for MOR hydrothermal circulation; however, fluid flow also is likely to occur parallel to spreading ridges since this is the dominant orientation of ridge flank faults and cracks. At the JdF SR site, basement fluid is younger and less chemically altered than crustal fluid samples closer to the ridge axis, suggesting a local source of recharge [*Elderfield et al.*, 1999; *Wheat et al*., 2000]. The fluid flow hypothesis at SR proposes an along-strike hydrothermal flow (SW-to-NE) controlled by several major volcanic outcrops (seamounts) exposed through the sediment cover [*Mottl et al*., 1998; *Wheat et al*., 2000; *Hutnak et al*., 2006; *Newman et al*., 2010; *Wheat et al*., 2010]. The seamounts' origins are not known with certainty, but these features are most likely a product of off-axis volcanism superimposed on a pre-existing elongated high in the

volcanic basement that likely is a fault-bounded abyssal hill underlying and connecting the locations of the seamounts and the SR boreholes. The exposed outcrop areas range from 0.5 km^2- 9.6 km^2 [*Hutnak et al.*, 2006]. There are three main pieces of evidence that support this hypothesis: (1) The discovery of hot springs venting from Baby Bare, (2) increased chemical alteration of fluids from SW to NE, and (3) increased radiocarbon ages of fluid from SW to NE on Second Ridge.

(1) In 1995, an expedition using the DSV *Alvin* discovered hot springs venting near a summit fault along Baby Bare. The fluid was measured at 25° C and supported several thysirid clam communities. While this discovery does not directly indicate fluid flow *direction* at SR, it does confirm hydrothermal discharge occurring only 2 km SW of the borehole array.

(2) This same expedition sampled the fluid seeping from Baby Bare and in another study compared its chemical composition to that of bottom seawater, sediment pore fluid, basement fluid from the most northern borehole 1026B, and fluid from Mama Bare to the north [*Wheat et al.*, 2000]. Given enough time and heat, basement fluid will appear chemically distinct from cold recharging seawater as ion-exchange occurs within the surrounding basalt (e.g. fluid decrease/crust increase in [Na^+], [Mg^{2+}], [SO_4^{2-}], [NO_3^-] and fluid increase/crust decrease in [Ca^{2+}], [Sr^{2+}], and [B^{3+}]) [*Wheat and Mottl*, 2000]. The study concluded a ridge-parallel hydrothermal fluid flow from SW-to-NE based on increasing geochemical alteration towards the NE.

(3) A more recent study sampled basement fluid discharging through Baby Bare and northern Hole 1026B. Mean radiocarbon ages of 11,890 ybp and 13,010 ybp,

respectively, were measured that also is consistent with a flow from southwest to northeast, as the age of hydrothermal fluid increases with time residing in basement [*Walker et al*., 2008]. This age increase indicates a flow rate of 5.7 m/yr. However, ridge-flank fluids with highly depleted $\delta^{13}C$ were observed, and the study concluded a strong carbon removal process must be present for this to occur. This inference is supported by the decrease in dissolved inorganic carbon (DIC) concentrations. Local variability and possible sources of error for previously reported radiocarbon results [*Walker et al.*, 2008; *Sanford*, 1997] from JdF ridge flank fluids make it difficult to assess the robustness of this result and its interpretation.

Discharge sources and hydrothermal fluid flow direction have been hypothesized through previously stated means. However, the assumption that recharge occurs 52 km south of Baby Bare from Grizzly Bare remains unsubstantiated. Initially, Grizzly Bare was considered the recharge site due to low heat flow measurements across a sediment-basement transect aligning with SR [*Hutnak et al.*, 2006]. The most recently published study on Grizzly Bare, however, revealed a much more complex hydrological system. One of the several anomalies spotted was (1) radiocarbon ages of 10,000, 12,000, and 18,000 ybp in three of the four samples collected from boreholes sampling below the sediment-basement interface [*Wheat et al.*, 2013]. The other anomalies noted were (2) several high heat flow measurements of some transects (contrary to low heat values induced from recharge of cold bottom seawater), and (3) several ion species veering away from the

systematic trend that reflects some conservative mixing/reaction of fresh seawater with altered fluids [*Wheat et al.*, 2013].

D. Tracer Injection Experiment 2010

In the summer of 2010, a gas tracer injection experiment was performed for the first time in the ocean floor. Along with soluble metal salts (CsCl, $ErCl_3 \cdot 6H_2O$, $HoCl_3 \cdot 6H_2O$), fluorescent microspheres and stained bacteria, the gas sulfur hexafluoride (SF_6) was injected into one borehole in order to track the rate and direction of flow through this segment of the volcanic basement encompassed by the boreholes (**Figure 4, Table 1**). Sulfur hexafluoride is a stable inert gas that has been used in terrestrial hydrologic experiments as an ideal tracer because it does not occur naturally in significant amounts, does not react with the surrounding medium, and is relatively inexpensive [*Wilson and Mackay*, 1995; *Clark et al.*, 2004]. The use of an anthropogenic gas tracer in the ocean crust also reduces the possibility of other *in situ* SF_6 sources, such as those that have been found in volcanic spring water of terrestrial settings [*Busenberg and Plummer*, 2000]. A total of 23.3 mol of SF_6 was injected at the SR injection hole (1362B) over a period of about 20 hours while surface seawater was being pumped into the borehole at a mean pumping rate of 6.7 L/s [*Fisher et al.*, 2011]. Simple mass balance indicates that the mean injectate concentration was 47,600 nM.

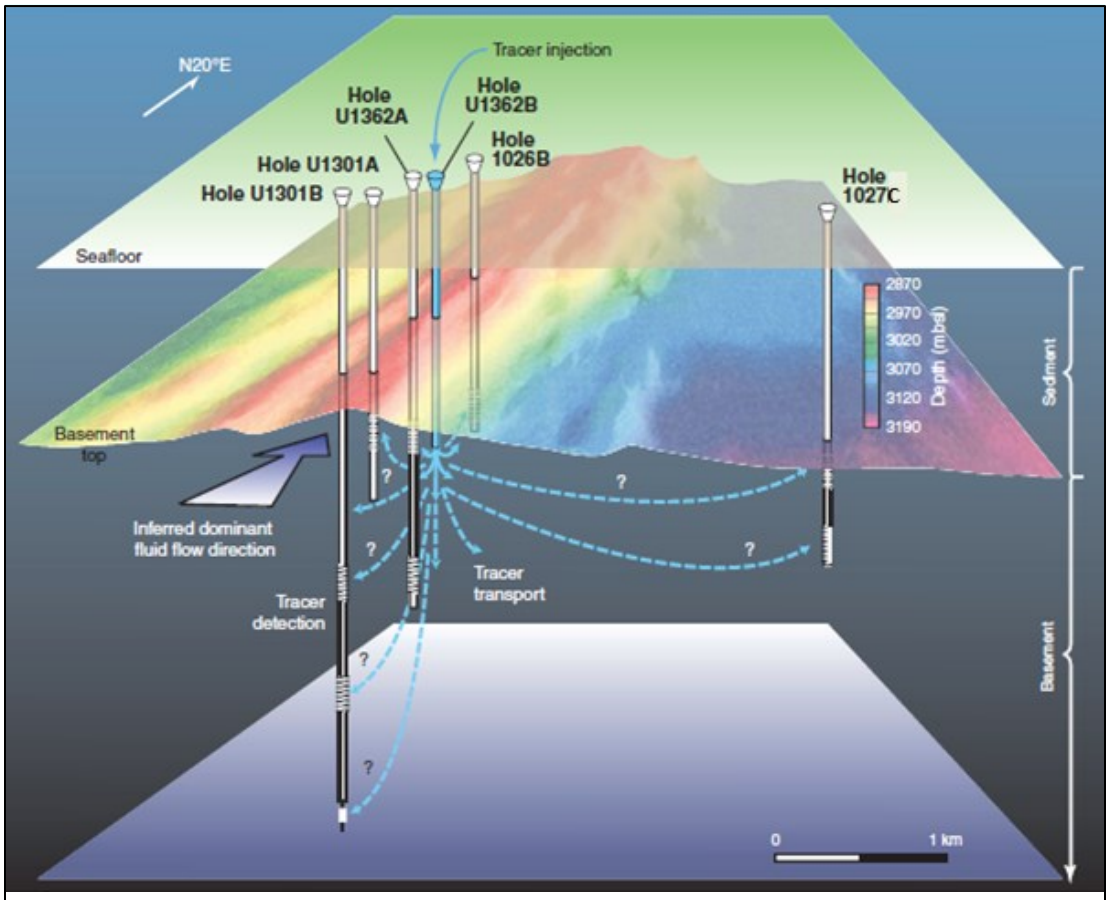

FIGURE 4. Cross-section of borehole observatory ("CORK"; see Fig. 5) array at SR. CORKs penetrate though sediment and into the upper volcanics at different depths. Injection at Hole 1362B showing possible flow paths. Modified from original figure drafted by Dr. James Cowen.

DISTANCE BETWEEN CORKs (m)	1026B	1362A	1362B	1027C	1301B	1301A
1026B		235	532	2199	1039	1076
1362A	235		311	2296	825	861
1362B	532	311		2322	514	550
1027C	2199	2296	2322		2446	2458
1301B	1039	825	514	2446		36
1301A	1076	861	550	2458	36	

TABLE 1. Relative distances between existing CORKs at SR in meters.

II. METHODS AND PROCEDURES

A. Sampling and Data Processing

The Circulation Obviation Retrofit Kit (CORK) system is a borehole plug created by the Ocean Drilling Program that allows researchers to monitor downhole parameters of the natural subseafloor by isolating the basement aquifer from the overlying ocean and sediments [*Becker and Davis*, 2005]. Typically, the borehole is cased through the sediment and open in a portion of the drilled upper basement (**Figure 5A**). In some CORKs, different sections of the basement are isolated using additional casing and packers. Each CORK carries a data logger that runs from the wellhead to the bottom of casing that can record pressure and temperature on an hourly basis and at multiple depths [*Becker et al*., 2005]. The most recent generation of CORKs are equipped to sip borehole fluid using osmotic samplers, commonly referred to as "osmosamplers" (OS). These can be attached to the wellhead or installed directly under the borehole in the open formation. Remote-operated vehicles (ROVs) and submersibles are used to service the CORKs, which include downloading of sensor data and retrieval/deployment of new OS (**Figure 5B**).

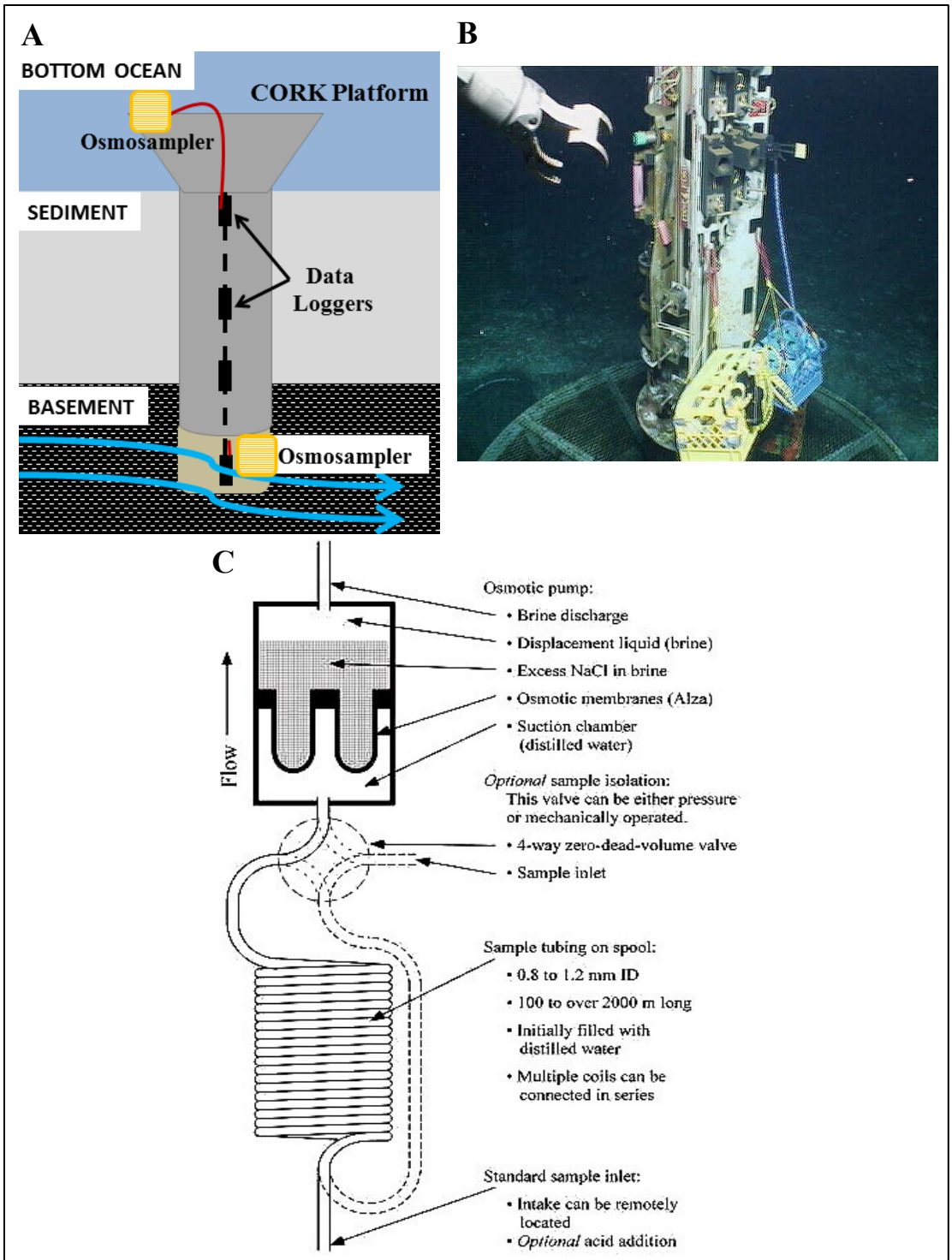

FIGURE 5. **[A]** General CORK design showing possible location of osmosamplers (wellhead or downhole). **[B]** *ROV* operations include switching OS and downloading sensor data. **[C]** The osmosampler design uses osmotic pressure to draw in bottom sea-water through a pre-filled freshwater spool [from *Jannasch et al.*, 2004].

Currently, only CORK 1026B is connected to the NEPTUNE Canada Cable Network. This allows live sensor data download and accessibility online, which is revolutionizing subseafloor hydrology research by allowing real time temperature and pressure data to be collected and analyzed instantly, particularly in response to seismic events.

Basement fluids for SF_6 analyses were collected using OS that takes advantage of osmotic pressure to draw in basement fluid through a 1.2 mm ID copper tube spool prefilled with distilled freshwater [*Jannasch et al*., 2004]. Because the saltwater reservoir is deployed with excess solid NaCl, it is hyper saline and once activated, maintains an osmotic driven flow across the membrane while simultaneously drawing in any fluid near the spool's end - in this case hydrothermal fluid in the basement (**Figure 5C**). The OS pump rate is proportional to the number of membranes and ambient basement temperature [*Jannasch et al*., 2004]. Once the spool is retrieved, it is sealed with pinch-off clamps and shipped to UCSB.

At UCSB, each coil is unraveled, cut into 1-meter lengths, and immediately sealed with steel pinch clamps on both ends. Once extractions are ready to begin, each 1-m long section is unclamped and ~12 cc N_2 (g) is injected from a syringe through the tubing directly into an evacuated vial (Vacutainer™), thereby minimizing possible air contamination. For every ten meters, three consecutive 1-m sections are set aside for SF_6 analysis; the remaining seven meters are sealed, labeled, and archived. The average volume of fluid extracted per 1-m sample was 1.11 mL and and average OS pump rate of 0.77 m/d. OS pump rate for each individual spool is

calculated by dividing the total length of hydrothermal fluid sampling by the known number of sampling days. The total interval of hydrothermal fluid collected is determined by locating the seawater-freshwater interface within each copper spool, i.e. the starting point of sampling. In the cases when the copper tube completely filled with saline water, the total volume pumped out was determined by measuring the salinity in the freshwater chamber so that a pump rate could be estimated.

Fluid samples were shipped to the Moss Landing Research Center where geochemical analyses pinpoint the start of hydrothermal sampling by examining the Cl concentration and the Ca/Na ratio. The Ca/Na ratio is used to distinguish hydrothermal (or basement) water from seawater, which can be drawn into the osmosamplers if a leak develops. Osmosamplers deployed for more than one year without service will keep sampling. Once the copper tubes are filled, the OS continues to pump and the initial samples are transferred into the freshwater chamber and are lost.

B. Analytical Methods

Fluid samples were analyzed via gas chromatography to determine SF_6 concentration. The gas chromatograph is equipped with a ^{63}Ni source electron capture detector (ECD). SF_6 analysis is based on the headspace method of *Wanninkhof et al.* [1987] and *Clark et al*. [2004]. Like *Clark et al*. [2004], Vacutainers™ are used as reaction vessels. After transferring, each container is filled with ultra-pure nitrogen gas and shaken for 3-5 minutes to equilibrate the SF_6, nitrogen, and water. According

to Henry's Law, approximately 98% of the dissolved SF_6 will partition into the headspace above, due to its low solubility and high headspace to water volume ratio in the containers. Assuming the pressure in the Vacutainer™ is ~ 1 atm after extraction, the following equation converts headspace molar fraction to water concentration in each sample:

$$C_w = \frac{[(V_{vac}-V_w) / V_w] * x_{hs}}{M_v} \quad \text{(Eq.2)}$$

where: C_w is the concentration of SF_6 in sample (mol/L); M_v is the molar volume of air at STP (22.4 L/mol); V_{vac} and V_w are, respectively, the initial volumes of vacutainer (mL) and of water sample (mL); and x_{hs} is the mole fraction of SF_6 in head space.

Calibration standards (146 pptv, 1.951 ppbv, and 10.05 ppbv certified by Scott-Marrin Inc.) were run before, during, and after each set of analyses and best fit-curves were calculated to obtain the mole fraction of SF_6 in the headspace (χ_{hs}). Samples that were above our highest standard of 10.05 ppbv, such as those from the injectate coil, were diluted in an additional vacutainer up to 1:4000, using a 10 µL, 50 µL, or 250 µL glass syringe. Mock extractions were performed in order to assess the integrity of the fluid extraction method. Deionized water was pumped into 1-m length copper tubes and clamped; the water was extracted, and then analyzed in the GC using methods previously stated. Mock extraction concentrations (C_w) of 0 − 0.01 nM were detected, a background concentration that is higher than current ambient air due to buildup of gas standards used at our lab. As such, all values detected at <0.01 nM

are considered below the detection limit of the SF_6 analytical method. Although the background values were relatively high, they still were more than three orders of magnitude lower than both the peak values observed in the basement fluid and more than 6 orders below the tagged injectate. The concentration of surface seawater in equilibrium with today's atmosphere ranges between 1-2 fM (0.000001-0.000002 nM) and deep ocean water typically contains < 0.02 fM (< 0.00000002 nM) [*Fine*, 2011].

Using the method developed for this project, our gas chromatograph had a detection limit and precision of 0.007 nmol/L and ± 0.9%, respectively. All subsequent data plotted reflect the mean value of three consecutive samples along with their standard deviation, with the exception of the corrected data for 1362B which plot two consecutive samples per point. The standard deviation of all plotted means was ±0.75 nM.

III. RESULTS

The following plots are either shown as SF_6 concentration vs. "distance along copper coil" or "days after injection". The term "southern" and "northern" holes refer to the location relative to injection Hole 1362B. A timeline of CORK operations and sampling intervals is outlined in **Figure 6**. All of our tracer data can be found in Appendix A.

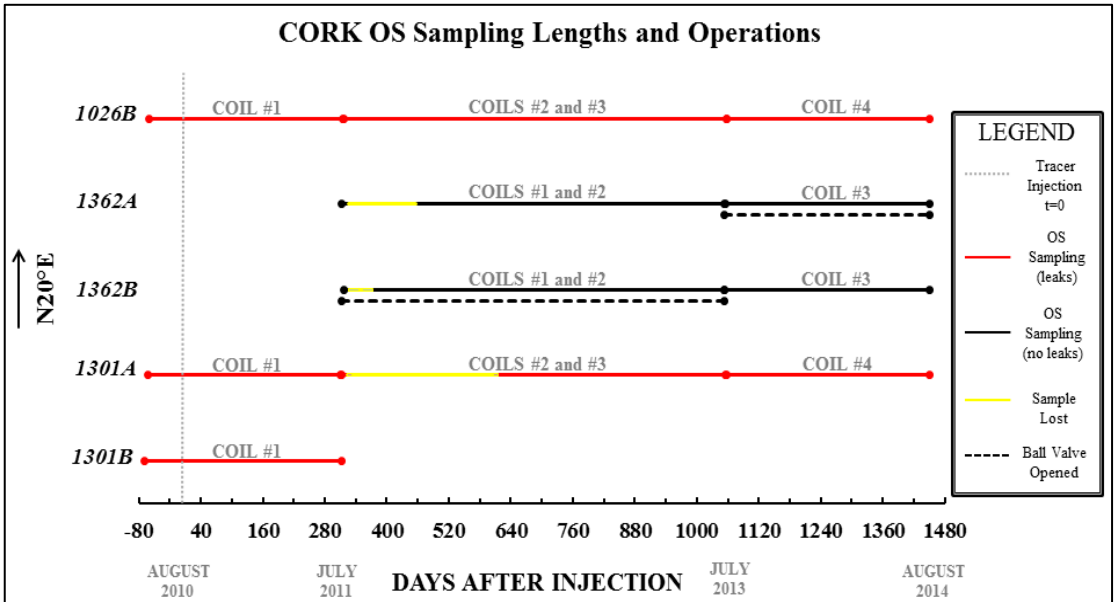

FIGURE 6. Gas OS sampling intervals of CORKs. Several OS were installed prior to injection (t=0, vertical dotted line), while others had OS installed approximately 1 year after injection. 1026B OS seawater-freshwater interface is not known but some sample was lost as was the case for all 2011 OS that were recovered in 2013.

A. Injectate Sampling

A fluid sampler was installed in CORK 1362B, during the tracer injection, to verify the timing and amount of injectate reaching the seafloor [*Fisher et al.*, *Proc. IODP*, Volume 327]. This particular osmosampler was designed to pump at a mean rate of 1-2 mL/hr - a much faster sampling rate than our long-term seafloor OS (1-2 mL/day). An SF_6 peak arrival time at ~15 m and an average concentration of 35.6 µM is seen (**Figure 7**), very close to the mean concentration calculated by mass balance (47.6 µM). According to this estimate, at least ~75% of the injectate entered the formation. However, this mean estimate does not include the first 15 m, as these samples were above our maximum detection limit. This estimate serves as a known

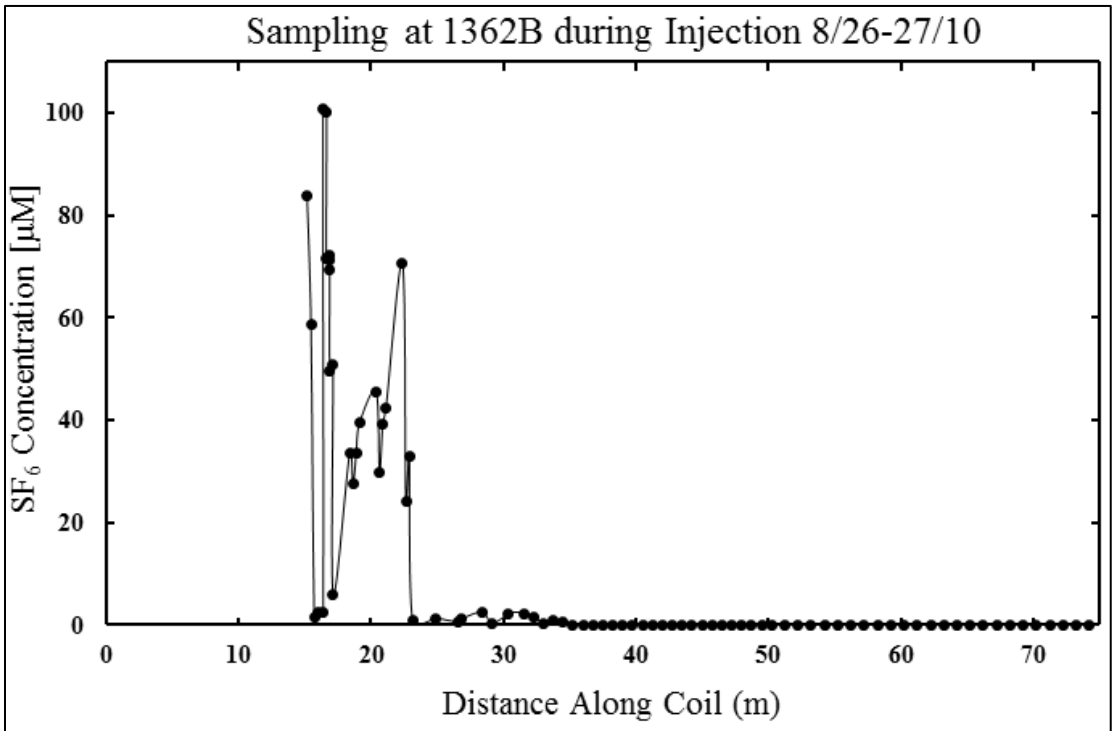

FIGURE 7. A copper spool was installed at 1362B prior to the 24-hr injection experiment, collecting injectate as it passed into the formation. Mean concentration at 35 µM. Samples from 0 m-15 m were above our detection limit.

minimum captured, although lack of a finer sampling resolution along the copper tube, and/or analytical precision in diluted samples is possible.

B. CORK Wellhead Sampling

Southern CORK 1301B, located 515 m SW of 1362B, was drilled 318 meters into basement (mib). Hole 1301B had an OS installed two months prior to injection and was recovered in summer 2011 along with OS at 1301A. Concentrations are < 0.01 nM, very close to the detection limit. This is consistent with fluid analyses confirming a non-hydrothermal signature from the Ca/Na ratio. Pump malfunction is suspected, and therefore no interpretations can be made for 1301B [*Geoff Wheat*,

personal comm.]. Furthermore, new osmosamplers were not installed on this CORK during the summer 2011 recovery.

Southern CORK 1301A was installed during IODP Expedition 301 in 2004. It is located 550 SW of Hole 1362B and was drilled 108 meters in basement (mib) and cased between the seafloor and 15 mib. Samplers at 1301A are located on the wellhead above, and the fluid sampling intake line extends to just below the casing. Osmosamplers were recovered and replaced in 2011 and 2013. Due to an unexpected delay of our 2012 research expedition, second and third coils were recovered in summer 2013. As a result, about 295 days of sampling was lost as pumping can only be stopped upon arrival on deck. Results show an SF_6 plume arriving at day 262 with a peak arrival of 22±11 nM at 305 days after injection (**Figure 8**). In the second coil (day 606 through 831), concentrations rapidly decrease from 0.02 nM to the detection limit beginning in day 617. Due to the data gap, the record does not capture the entire SF_6 signal as the plume migrates away from 1301A. SF_6 detections disappear by the third coil (day 831 to 1047) except for two points above the detection limit of 0.01 nM.

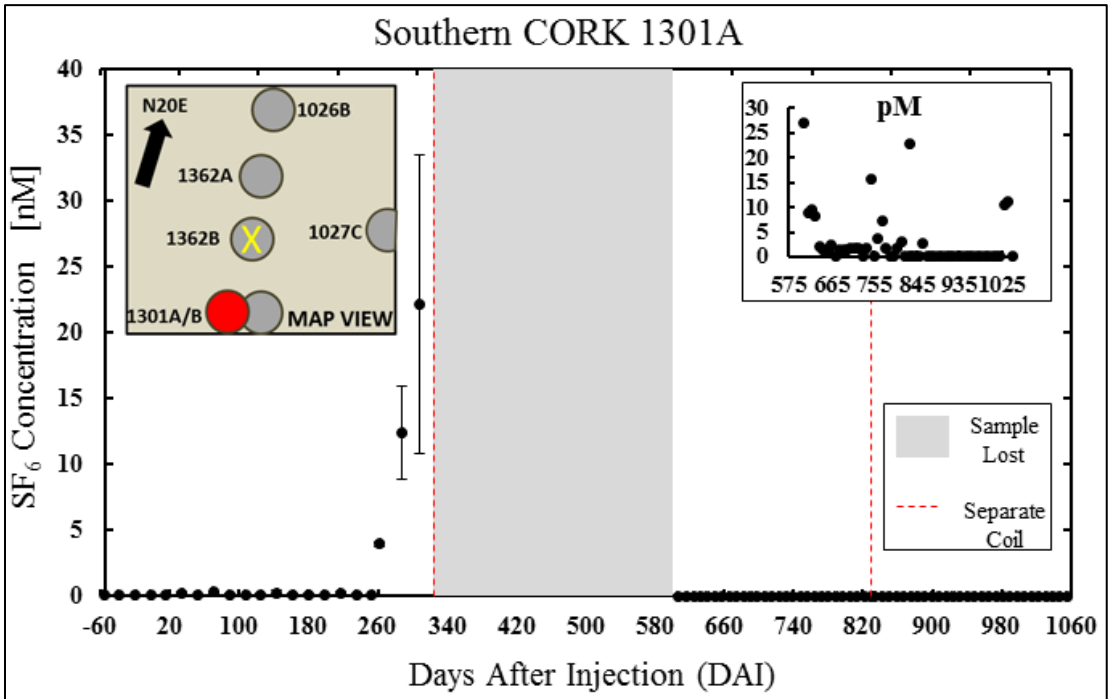

FIGURE 8. A SF_6 first peak arrival is observed at 1301A, 550 m SW of 1362B, at ~305 DAI. About 295 days of sampling were lost due to unexpected delay of OS recovery. Plume tail can be seen at the start of sampling (coil 2, day 575), with concentrations gradually disappearing by third coil (red dashed line, right).

CORK 1362B was drilled 110 mib and cased 70 mib during IODP Expedition 327. It was sealed immediately following the 24-hr injection experiment. This hole, along with 1362A, is hydrologically stable, i.e. not leaking. Hole 1362B was not deployed with wellhead OS in 2010 because the drill ship *JOIDES Resolution* was not equipped for these deployments [*Andrew Fisher, personal comm.*]. However, the drillship was able to deploy down hole samplers that were recovered in August 2014. In 2011 (313 DAI), wellhead OS were deployed after the ball valve was opened allowing basement water to vent into the overlying ocean. In 2013 (1053 DAI), the valve was closed and the well top OS replaced. Start of sampling at 1362B occurred at 313 DAI but about 47 days of sample were lost due to delayed recovery as also

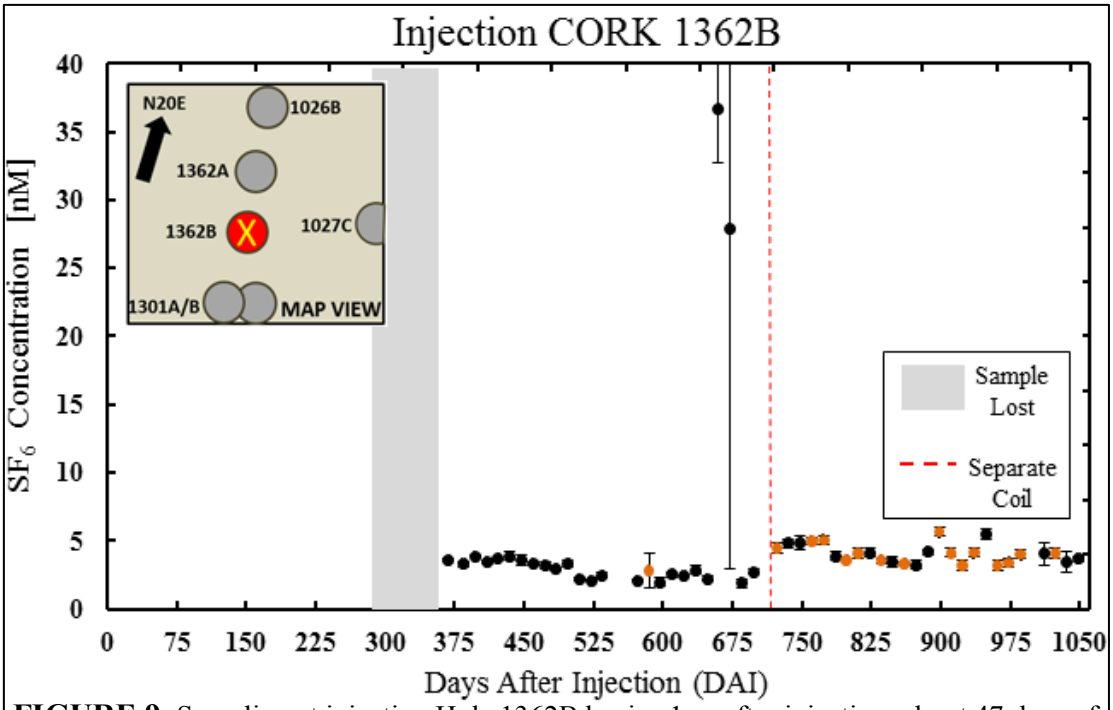

FIGURE 9. Sampling at injection Hole 1362B begins 1 yr after injection; about 47 days of sample were lost due to recovery delay. Mean concentration of the record was at ~4.6 nM. Orange points represent one sample with coil mean error plotted (1.26, 0.35 nM, respectively). All points have been corrected based on Ca^{2+} content.

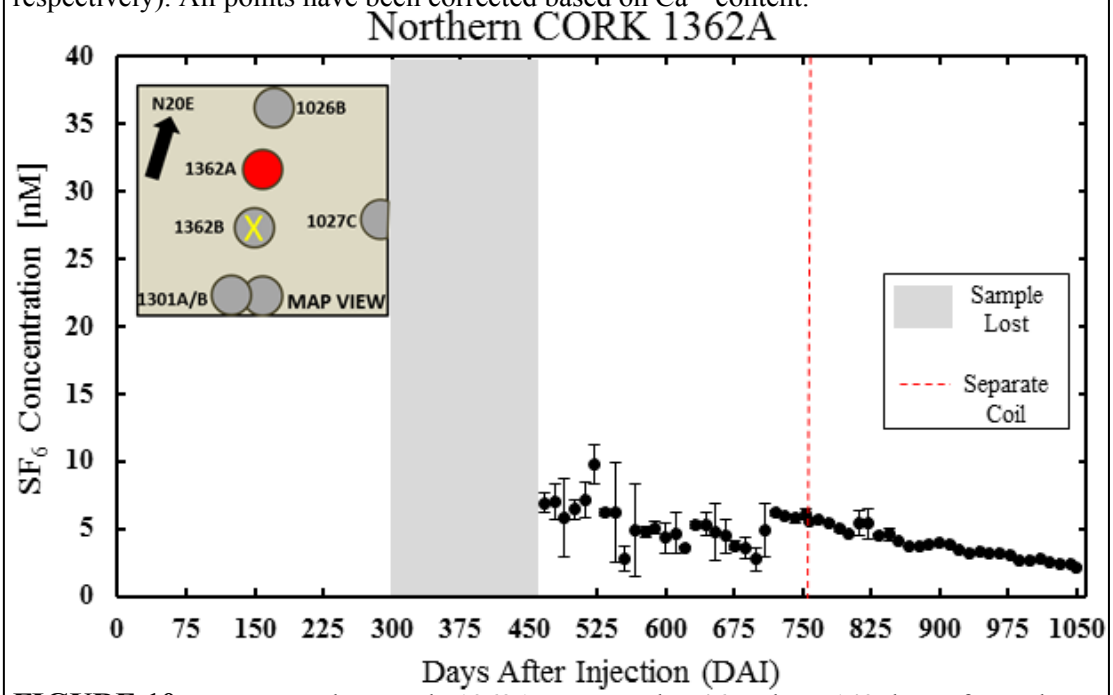

FIGURE 10. Data at northern Hole 1362A starts on day 467- about 143 days of sample was lost due to delay of OS recovery. The record mean concentration was at ~ 4.5 nM. Gradual decrease in concentration suggest plume slowly retreating away from 1362A.

occurred at 1301A (**Figure 9**). The maximum concentration (~ 40 nM) was observed at day 661 with a sustained mean concentration of ~ 4.6 nM from day 363 to day 1050 after injection.

CORK 1362A was drilled 292 mib and houses two distinct open basement intervals (shallow at 73 - 198 mib, deep at 198 - 292 mib). Sampling for copper OS occurred in the shallow interval with the sampling intake located at 73 mib. As with all samplers deployed in summer 2011, 1362A lost hydrothermal fluid from the start of the record; at this borehole, about 143 days were lost (**Figure 10**). No SF_6 peak is found in the record, although it is a possibility that it was present in the data gap that was over pumped. Fortunately, like 1362B, this CORK was deployed with a downhole sampler that was recovered in August 2014. The mean concentration for the entire sampling period was about ~ 4.5 nM, although the record is much noisier in the first 244 days of values from 466 DAI to 710 DAI (mean standard deviation of 1.09 nM) than for the remaining 300 days. The other interesting trend observed in 1362A is a gradual decrease in concentration as time goes on from about 6 nM to 2 nM at the end of the record.

The most northern hole, CORK 1026B, is an older borehole that was installed along with Hole 1027C during ODP Leg 168 in 1997 at the start of the ODP/IODP JdF project. Holes 1026B and 1027C were later upgraded and retrofitted with CORK observatories during IODP Expedition 301 in 2004. The casing penetrates 48 mib although the fluid sampling intake lines are located within the sediment interval (198 mbsf) due to a rubbly fill in the open basement interval. Although SF_6 concentrations

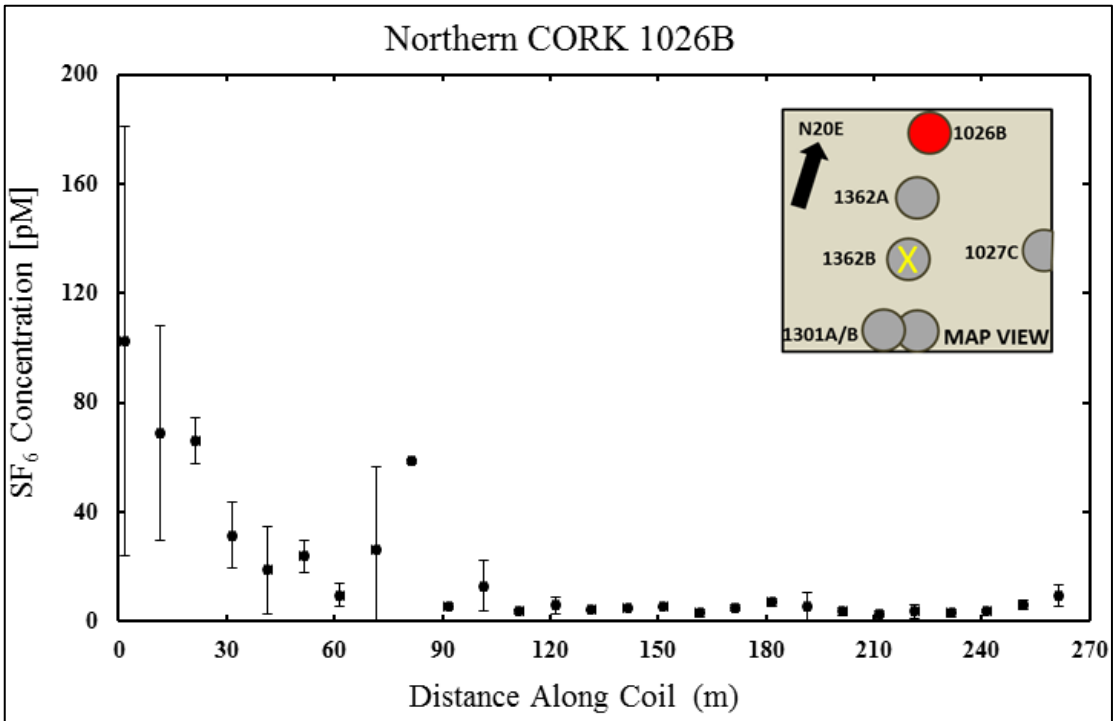

FIGURE 11. The SW-FW interface at most northern Hole 1026B, could not be established. Most recent end (July 2011) at x=0. SF_6 concentrations begin to rise above our detection limit (0m-81.5m) and can be interpreted to be plume arrival to the north. All fluid samples are diluted with SW based off of Ca/Na ratios. (1- 2% hydrothermal).

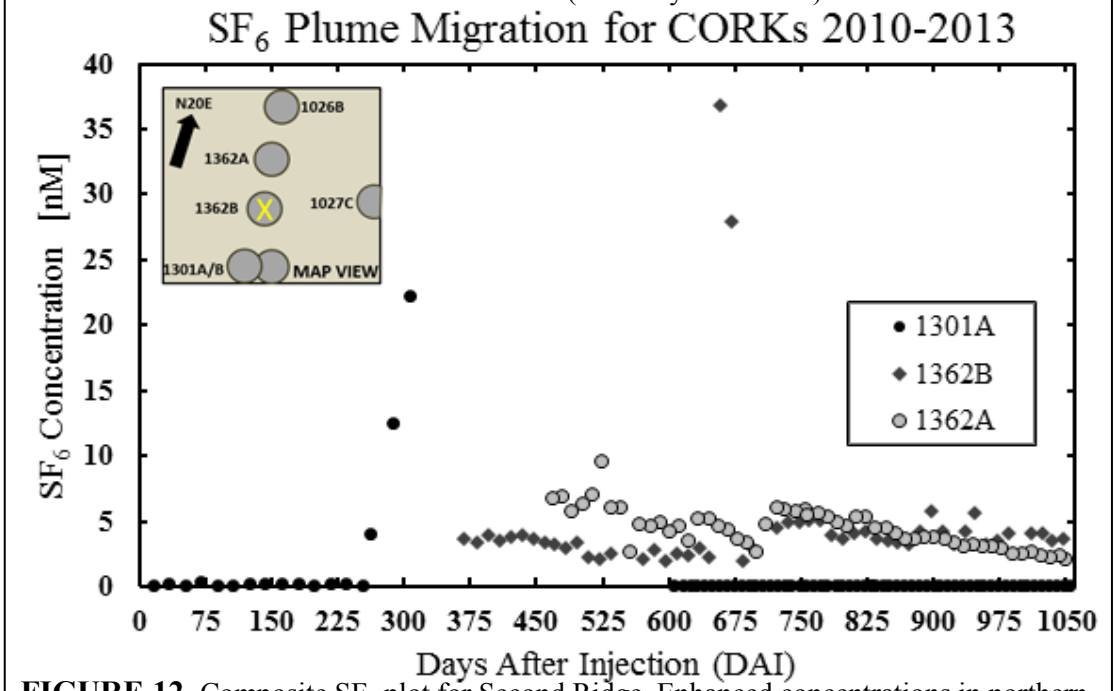

FIGURE 12. Composite SF_6 plot for Second Ridge. Enhanced concentrations in northern holes suggest a dominantly NE fluid flow direction, as hypothesized, with flow channeling of hydrothermal fluid through fractured basaltic matrix.

here are also close to the detection limit, an increase in concentration towards the most recent end of sampling is observed beginning at 81.5 m. Chlorinity and Ca/Na ratio data indicate the fluid sampled is only 1-2% hydrothermal with the remainder portion being seawater. Assuming an OS pump rate of 0.55 m/d (the pump rate observed at 1301A) and a dilution factor of 100, a first arrival at 1026B would occur at 166 DAI (**Figure 11**). This would imply the tracer arrived to the north before it did at 1301A, but we cannot say with certainty due to the leaky OS. Coils #2 and #3 were void of any SF_6 (**Figure 6**), although some of the sampling lost might have been the continuation of the SF_6 curve seen in Coil #1.

IV. DISCUSSION

A. Southern CORK 1301A

A composite plot of all viable SF_6 data (Holes 1301A, 1362B, 1362A) was generated to analyze the movement of SF_6 through SR for the three-year sampling period (**Figure 12**). A first peak arrival of tracer south of the injection source may contradict the NE fluid flow direction hypothesis [*Wheat et al.*, 2000] at a first glance, but we have substantial evidence that 1301A is leaking extensively. CORK 1301A is not sealed properly due to a casing seal being unavailable during its installation in 2004 [*Expedition 301 Scientists*, 2005]. This resulted in an inflow of cold bottom seawater into the hole and basement, as detected by pressure and temperature loggers [*Fisher et al.*, 2008]. Flow reversal began three years later and hydrothermal leakage is still occurring at an estimated rate of 2-5 L/s [*Winslow et al.*, 2013] despite efforts

to seal the casings with cement [*Wheat et al.*, 2010].

Tracer results from CORK 1301A yield an along-strike flow rate of 660 m/yr. This is the first time such a fast fluid velocity has been documented at the JdF eastern flank, about two orders of magnitude higher than previous estimates. If permeability anisotropy is the main cause of this rapid hydrothermal flow, then all low-end flow rates previously estimated may be reconciled. Permeability anisotropy can be prevalent in the igneous ocean crust due to the nature of faulting/layering imposed by the tectonics of a mid-ocean ridge setting [*Fisher*, 1998; *Fisher*, 2004]. A heterogeneous, fractured aquifer system is not unrealistic in the upper ocean crust, which is typically comprised of multiple extrusive layers of basaltic rubble, pillow lava flows, and massive lava flows, cut by ridge axis-parallel faults. Molecular diffusion/mixing can occur from distinct fluid flow zones to the surrounding stagnant layers, such as the overlying sediment or more impermeable massive lava flow deposits [*Stein and Fisher*, 2003]. A correction factor of 2-50 has been suggested at this particular site [*Fisher*, 2004]. *Sanford* [1997] concluded that if molecular diffusion is more dominant than dispersion in fractured volcanic rock, corrections of 10-1,000x should be applied to fluid velocity estimates derived from geochemical tracers. Using the lateral flow rate of 5.7 m/yr estimated by *Walker et al.* [2008], a diffusion- correction of 10-1,000 would yield an adjusted flow rate of 57- 5,700 m/yr. Alternatively, applying the same correction to the 1-3 m/yr estimate based on geochemical tracers from the *Elderfield* [1999] study would result in an adjusted flow rate range of 10-3,000 m/yr. *Stein and Fisher* [2003] calculated a model-derived flow

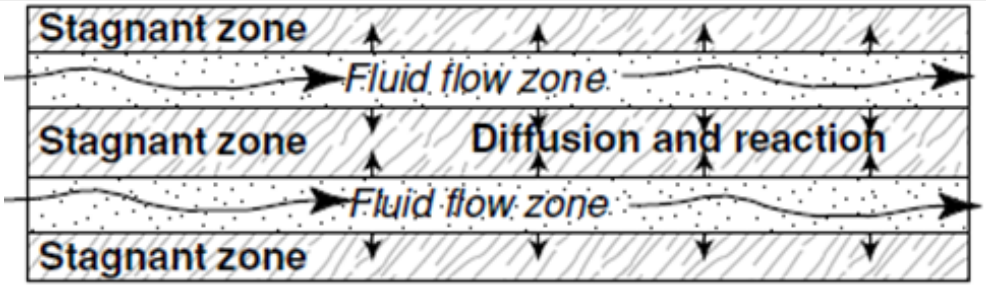

FIGURE 13. Based on our tracer study, fluid flow in the upper crust at SR seems to move through isolated, connected fractures that make up only a small portion of the crustal structure. Diffusion/mixing of old pore-water residing in aquiducts also turn out to be dominant - a concept that has not been incorporated in previous velocity/age estimates [from *Fisher*, 2004].

rate of 12-4,000 m/yr in order to match seafloor heat flow observations in the region - a range which is justified by anisotropy, and is very similar to previous corrected estimates.

As previously mentioned, recent studies have hypothesized that anisotropy may be a cause for the variability seen in hydrological estimates [*Winslow et al.*, 2013; *Fisher et al*., 2008; *Fisher*, 2004; *Stein and Fisher*, 2003; *Bethke and Johnson*, 2002; *Nehlig and Juteau*, 1998; *Tsang and Neretnieks*, 1998]. It has also been suggested that rapid lateral flow is required to sustain the isothermal basement temperatures observed at SR [*Fisher*, 1998]. The idea that fluid flow in heterogeneous, anisotropic upper ocean crust is variable and potentially rapid finally has been tested by conducting this multi-hole tracer experiment. Our tracer-derived flow rate of 660 m/yr falls within *all* three molecular diffusion-corrected flow rate estimates, specifically, within two orders of magnitude. Directly observing a rapid flow rate that falls within the range of estimates does support the hypothesis of anisotropic flow within the ridge flank. The upper extrusive basement at SR can be

envisioned as an aquitard-dominated porous media where connected fractures govern fluid flow along with diffusive exchange/mixing between distinct layers (**Figure 13**), as evidenced by the much faster SF_6 velocities compared to radiocarbon and geochemically-derived estimates [*Bethke and Johnson*, 2002].

B. CORKs 1362B and 1362A

CORKs 1362B/A did not sample basement fluid for the first 313/456 days after tracer injection. As a result, crucial data such as plume arrival and flow rate cannot be determined with confidence with the present data set. It is hoped that this data gap will disappear after their downhole samples collected in summer 2014 are analyzed. Nevertheless, since sampling began for both CORKs, which are located 311 meters apart, the largest amount of tracer was observed here. Hydrothermal basement-water SF_6 concentrations were three orders of magnitude higher than our methodological background detection limit. This may be consistent with a dominantly NE fluid flow, as hypothesized from prior studies.

Injection Hole 1362B is the most consistent of the records generated. With the exception of an SF_6 peak at ~ 661 DAI, the record is surprisingly steady. The mean concentration was ~ 4.6 nM with the lowest value ~1.9 nM, between the detection limit (0.01 nM) and the injectate concentration (about 50,000 nM). The fact that there is a multi-year persistence of tracer stationary at 1362B suggests that only a small fraction of the rock matrix is hydrologically occupied, which is characteristic of anisotropy and flow channeling [*Stein and Fisher*, 2003; *Tsang and Neretnieks*, 1998]. Flow channeling through a heterogeneous rock is a pressure-driven flow

system in which fluid follows the path of least resistance (small cracks/fractures) and can be seen graphically as multiple peaks and/or long tails [*Tsang and Neretnieks*, 1998]. IODP core analysis of hole 1362B is minimal, as coring was not possible due to injection taking place before CORK installation, and because the basement around 1362B was documented as rubbly and unstable [*Fisher et al.*, 2011]. CORK 1362B was also part of a free flow experiment where a large diameter ball-valve was opened at ~ 313 DAI and hot shimmering fluid discharged at a rate of 5-10 L/s [*Fisher et al.*, 2011]. So, it is possible that the tracer plume moved away from the borehole for a year only to return after the valve was opened.

Hole 1362A has somewhat comparable characteristics in that it has a similar mean concentration (~4.5 nM). However, there is more variability (mean standard deviation of 1.09 nM) in values for the first 244 days of analyzed samples as compared to the latter half of the record. The possibility for this noise being caused by laboratory procedures is unlikely, as the consistently decreasing values precede the end of the first coil (dotted red line in **Figure 9**). The tracer concentration does not waver below 1.7 nM, a value similar to 1362B's minimum of 1.9 nM. The variability seen in the 1362A record can be interpreted as multiple SF_6 peaks, which indicate heterogeneous flow paths [*Tsang and Neretnieks*, 1998], as tracer makes its way to the hole from different locations, and possibly different depths, through the basement at SR. Towards the latter half of the record (~710 DAI to 1054 DAI), concentrations gradually decrease threefold. IODP core logging reports indicate that pillow basalts are the most dominant structure found at 1362A. Among the other characteristics

found in 1362A rock samples were moderate vesicular textures, moderate to high hydrothermal alteration, secondary mineral filling in vesicles, and uniformly distributed vertical extensional structures [*Fisher et al.*, 2011]. The report indicates "more complex hydrothermal processes" taking place and a higher fracture/vein intensity in the pillow basalts than in the sheet flows.

Although fluid flow direction and velocity have been estimated, hydrological permeability based on our gas tracer experiment remains pending for this site. Because of the inherently complex nature of a fractured basaltic matrix, flow paths are heterogeneous and currently unpredictable, as seen from multiple tracer peaks (or lack thereof). Also, hydrological flow at SR is governed by pressure and buoyancy, and a Darcian-derived permeability is not applicable. However, one can calculate a volumetric flow rate based on borehole temperature data which will yield permeability using a radial diffusive equation [*Fisher et al*., 1997]. Currently, only two of the existing CORKs are working properly for this to be achieved, and no published estimates using this method have been made as of yet. With the recovery of pressure/temperature data at both 1362A and 1362B in 2013 and 2014, there should be enough information to calculate effective bulk permeability at SR.

V. CONCLUSIONS AND IMPLICATIONS

The tracer experiment at Second Ridge was successful in injecting a substantial amount of SF_6 into the subseafloor and documenting its transport over the course of three years. Although a few of the CORK observatories operated as

intended, we were still able to detect, interpret and confirm a probable dominant northeasterly fluid flow direction as well as estimate a fluid velocity through the buried ridge. The fact that multiple valves were opened and closed during the experiment and some of the pre-existing CORKs were leaking makes it harder to confirm flow direction because the natural state of the SR aquifer is disturbed. Permeability estimates were not possible to acquire based on our tracer data, but future work using other existing CORK data (temperature, pressure) can help resolve effective permeability in SR.

Results from this study indicate a maximum lateral flow rate of 660 m/yr, an estimate indicating that the hydrogeological fabric of the upper volcanic zone at SR is mostly heterogeneous and anisotropic, as speculated in previous studies. This also is consistent with IODP drilling reports of a rubbly, highly fractured basement, which is typical in upper oceanic crustal settings. Although tracer was initially detected south of the injection, this may be due to unintentional leaks. Most of the tracer remains towards the northern end of the array. This is consistent either with along-strike basement fluid flow from SW to NE, as previously hypothesized, or with hovering of a spreading SF_6 plume. Future work would greatly benefit from sampling at all exposed seamounts for SF_6-tagged crustal fluid, to unequivocally determine direction of flow from the tracer injection site.

Previous hydrological estimates have relied heavily on groundwater modeling that assume homogeneous and isotropic conditions in the upper ocean crust, an assumption that is questionable for a tectonically and thermally evolving ridge flank

system [*Fisher*, 1998]. If anisotropy is more widespread than previously thought, hydrothermal residence times are considerably shorter than currently estimated - on the scale of weeks to years. This could have vast implications in the way we envision heat, fluid, and mineral exchange between the crustal reservoir and ocean.

REFERENCES (Page 1)

Alt, J.C. (1995). "Subseafloor Processes in Mid-Ocean Ridge Hydrothermal Systems." *Geophysical Monograph Series*, *Volume 91*, pp. 84-115.

Alt, J.C., D.A.H. Teagle. (2003). **"**Hydrothermal alteration of upper oceanic crust formed at a fast-spreading ridge: mineral, chemical, and isotopic evidence from ODP Site 801." *Chemical Geology*, *Volume 201, Number 3-4***,** pp. 191-211.

Bach, W., J.C. Alt, Y.L. Niu, S.E. Humphris, J. Erzinger, H.J.B. Dick. (2001). "The geochemical consequences of late-stage low-grade alteration of lower ocean crust at the SW Indian Ridge: Results from ODP Hole 735B (Leg 176)." *Geochimica et Cosmochimica Acta Volume 65, Number 19,* pp. 3,267-3,287.

Becker, K., E.E. Davis. (2005). "A review of CORK designs and operations during the Ocean Drilling Program." *In* Fisher, A.T., Urabe, T., Klaus, A., and the Expedition 301 Scientists, *Proc. IODP,* 301: College Station TX (Integrated Ocean Drilling Program Management International, Inc.)

Becker, K.*,* A.T. Fisher. (2008). "Borehole packer tests at multiple depths resolve distinct hydrologic intervals in 3.5-Ma upper oceanic crust on the eastern flank of Juan de Fuca Ridge" *Journal of Geophysical Research., Volume 113,* pp. B07105.

Benjamin, S.B., R.M. Haymon. (2006). "Hydrothermal mineral deposits and fossil biota from a young (0.1 Ma) abyssal hill on the flank of the fast spreading East Pacific Rise: evidence for pulsed hydrothermal flow and tectonic tapping of axial heat and fluids." *Geochemistry, Geophysics, Geosystems, Volume 7, Number 26,* pp.Q05002.

Bethke, C.M., T.M. Johnson. (2002). "Paradox of groundwater age: Correction" *Geology, Volume 30, Number 4*, pp. 385-388.

Bischoff, J.L., F.W. Dickson. (1975). "Seawater-basalt Interaction at 200°C and 500 Bars: Implications for Origin of Seafloor Heavy Metal Deposits and Regulation of Seawater Chemistry." *Earth and Planetary Science Letters, Volume 25,* pp. 385-397.

Busenberg, E.*,* L.N. Plummer. (2000). "Dating young groundwater with sulfur hexafluoride: Natural and anthropogenic sources of sulfur hexafluoride"*, Water ResourcesResearch, Volume 36, Number 10,* pp. 3,011-3,030.

Carbotte, S.M. (2001). "Mid-Ocean Ridge Seismic Structure." in *Encyclopedia of Ocean Sciences. Academic Press*, pp. 1,788-1,798.

Carbotte S.M., J.P. Canales, M.R. Nedimović, H. Carton, J.C. Mutter. (2012). "Recent Seismic Studies at the East Pacific Rise 8°20'-10°10'N and Endeavour Segment: Insights into Mid-Ocean Ridge Hydrothermal and Magmatic Processes." *Oceanography*, *Volume 25*, *Number 1*, pp. 100-112.

REFERENCES (Page 2)

Clark, J.F., G.B. Hudson, Davisson, M.L. G. Woodside, & R. Herndon. (2004). "Geochemical imaging of flow near an artificial recharge facility, Orange County California." *Ground Water, Volume 42*, pp.167-74.

Davis, E.E., C.R.B. Lister, U.S. Wade, R.D. Hyndman. (1980). "Detailed heat flow measurements over the Juan de Fuca Ridge System" *Journal of Geophysical Research: Solid Earth, Volume 85*, pp. 299-310.

Davis, E.E., K. Wang, R.E. Thompson, K. Becker, J.F. Cassidy. (2001). "An episode of seafloor spreading and associated plate deformation inferred from crustal fluid pressure transients." *Journal of Geophysical Research, Volume 106*, *Number B10*, pp.21,953-21,963.

Davis, E.E., A. LaBonte, J. He, K. Becker, A. Fisher. (2010). 'Thermally stimulated "runaway" downhole flow in a superhydrostatic ocean crustal borehole: Observations, simulations, and inferences regarding crustal permeability', *Journal of Geophysical Research, Volume 115*, pp. B07102.

Elderfield, H., C.G. Wheat, M.J. Mottl, C. Monnin, B. Spiro. (1999). "Fluid and geochemical transport through oceanic crust: A transect across the eastern flank of the Juan de Fuca Ridge." *Earth and Planetary Science Letters, Volume 172, Number 1,*. 151-165.

Expedition 301 Scientists. (2005). "Site U1301". *In* Fisher, A.T., Urabe, T., Klaus, A., and the Expedition 301 Scientists, *Proc. IODP, 301: College Station TX (Integrated Ocean Drilling Program Management International, Inc.).* doi:10.2204/iodp.proc.301.106.2005

Fine, R.A. (2011). "Observations of CFCs and SF_6 as ocean tracers" *Annual Review, Marine Science*, *Volume 3,* pp. 173-195.

Fisher, A.T., K. Becker, E.E. Davis. (1997). "The permeability of young oceanic crust east of Juan de Fuca Ridge, as determined using borehole thermal measurements." *Geophysical Research Letters*, *Volume* 24, pp. 1,311-1,314.

Fisher, A.T. (1998). "Permeability within basaltic oceanic crust" *Reviews of Geophysics, Volume 36*, *Number 2,* pp. 143-182.

Fisher, A.T., E.E. Davis, M. Hutnak, V. Spiess, L. Zühlsdorff, A. Cherkaoui, L. Christiansen, K. Edwards, L. Macdonald, H. Villinger, M.J. Mottl, G.C. Wheat, K. Becker. (2003). "Hydrothermal recharge and discharge across 50 km guided by seamounts on a young ridge flank." *Nature*, *Volume 421*, pp. 618-622.

REFERENCES (Page 3)

Fisher, A.T. (2004). "Rates and patterns of fluid circulation", in *Hydrogeology of the Oceanic Lithosphere,* edited by E. E. Davis and H. Elderfield, pp. 339-377, Cambridge Univ. Press, New York.

Fisher, A.T., E.E. Davis, K. Becker. (2008). "Borehole-to-borehole hydrologic response across 2.4 km in the upper oceanic crust: Implications for crustal-scale properties", *Journal of Geophysical Research, Volume 113*, pp. B07106.

Fisher, A.T., J. Cowen, C.G. Wheat, J.F. Clark. (2011). "Preparation and injection of fluid tracers during IODP Expedition 327, eastern flank of Juan de Fuca Ridge." *In* Fisher, A.T., T. Tsuji, K. Petronotis, and the Expedition 327 Scientists*, Proc. IODP, 327: Tokyo (Integrated Ocean Drilling Program Management International, Inc.). doi:10.2204/iodp.proc.327.108.2011*

Haymon, R.M., D.J. Fornari, M.H. Edwards, S. Carbotte, D. Wright, K.C. Macdonald. (1991). "Hydrothermal vent distribution along the East Pacific Rise Crest (9°09'–54'N) and its relationship to magmatic and tectonic processes on fast-spreading mid-ocean ridge." *Earth and Planetary Science Letters Volume 104*, pp. 513-534.

Haymon, R.M. (1996). "The response of ridge crest hydrothermal systems to segmented, episodic magma supply" *In*: MacLeod, C.J., Tyler, P., and Walker, C.L. (eds.), *Tectonic, Magmatic, Hydrothermal, and Biological Segmentation of Mid-Ocean Ridges, Geological Society of London Special Publication No. 118*, pp.157-168.

Hutnak, M., A.T. Fisher, L. Zühlsdorff, V. Spiess, P.H. Stauffer, C.W. Gable. (2006). "Hydrothermal recharge and discharge guided by basement outcrops on 0.7–3.6 Ma seafloor east of the Juan de Fuca Ridge: Observations and numerical models." *Geochemistry, Geophysics, Geosystems, Volume* 7, pp. Q07O02.

Jannasch, H.W., G.C. Wheat, J.N. Plant, M. Kastner, D.S. Stakes. (2004). "Continuous chemical monitoring with osmotically pumped water sampler: OsmoSampler design and applications." *Limnology and Oceanography: Methods*, *Volume 2*, pp. 102-113.

Johnson, H.P., M. Pruis. (2003). "Fluxes of fluid and heat from the oceanic crustal reservoir." *Earth and Planetary Science Letters*, *Volume 216*, pp. 565-574.

Lister, C.R.B. (1972). "On the Thermal Balance of a Mid-Ocean Ridge." *Geophysical Journal of the Royal Astronomical Society*, *Volume 26*, pp. 515-535.

Macdonald, K.C., P.J. Fox, R.T. Alexander, R. Pockalny, P. Gente. (1996). "Volcanic growth faults and the origin of Pacific abyssal hills." *Nature, Volume 380*, pp. 125-129.

Macdonald, K.C. (2001). "Seafloor Spreading: Mid-Ocean Ridge Tectonics", in *Encyclopedia of Ocean Sciences (eds. J. Steele, S. Thorpe, K. Turekian), Academic Press,* pp. 1,798-1,813.

REFERENCES (Page 4)

Mottl, M.J., C.G. Wheat. (1994). "Hydrothermal circulation through mid-ocean ridge flanks: Fluxes of heat and magnesium", *Geochimica et Cosmochimica Acta*, *Volume 58, Issue 10*, pp. 2,225-2,237.

Mottl, M.J.**,** C.G. Wheat, E. Baker, N. Becker, E. Davis, R. Feely, A. Grehan, D. Kadko, M. Lilley, G. Massoth, C. Moyer, F. Sansone. (1998). "Warm springs discovered on 3.5 Ma oceanic crust, eastern flank of the Juan de Fuca Ridge." *Geology*, *Volume 26*, pp**.** 51-54.

Nehlig, P., T. Juteau. (1988). "Deep crustal seawater penetration and circulation at ocean ridges: Evidence from the Oman Ophiolite" *Marine Geology*, *Volume 84*, pp. 209-228.

Newman, K., M.R. Nedimović, J.P. Canales, S.M. Carbotte. (2011). "Evolution of seismic layer 2B across the Juan de Fuca Ridge from hydrophone streamer 2-D traveltime tomography." *Geochemistry ,Geophysics, Geosystems*, *Volume 12*, *Number 5*.

Sanford, W.E. (1997). "Correcting for diffusion in carbon-14 dating of ground water" *Ground Water*, *Volume 35*, pp. 357-361.

Staudigel, H., S.R. Hart, S. Richardson. (1981). "Alteration of the oceanic crust: Processes and timing." *Earth Planetary Science Letters*, *Volume 52,* pp. 311-327.

Stein, C. A., S. Stein. (1994). "Constraints on hydrothermal heat flux through the oceanic lithosphere from global heat flow" *Journal of Geophysical Research*, *Volume* 99, *Number* B2, pp. 3,081-3,095.

Stein, C.A., S. Stein, A.M. Pelayo. (1995). "Heat Flow and Hydrothermal Circulation." *Geophysical Monograph Series*, *Volume 91*, pp. 425-445.

Stein, J. S., A.T. Fisher. (2003). "Observations and models of lateral hydrothermal circulation on a young ridge flank: Numerical evaluation of thermal and chemical constraints" *Geochemistry, Geophysics, Geosystems*, *Volume 4, Number 3*.

Sverdrup, Keith, A.C. Duxbury, A.B. Duxbury. (2004). "*Introduction to the World's Oceans*". McGraw-Hill Publishing Company. *Chapter 4*.

Till, C.B., Grove, T.L., A.C. Withers. (2012). "The beginnings of hydrous mantle wedge melting." *Contributions to Mineralogy and Petrology, Volume 163, Number 4,* pp. 669-688.

Tsang, C., I. Neretnieks. (1998). "Flow channeling in heterogeneous fractured rocks" *Reviews of Geophysics, Volume 36, Number 2*, pp. 275-298.

REFERENCES (Page 5)

Von Damm, K.L. (1995). "Controls on the chemistry and temporal variability of seafloor hydrothermal fluids", in *Seafloor Hydrothermal Systems: Physical, Chemical, Biological, and Geological Interactions*, *Geophysical Monograph Series*, *Volume 91*, edited by S. E. Humphris et al., pp. 222-247.

Von Damm, K.L. (2004). "Evolution of the Hydrothermal System at East Pacific Rise 9°50'N: Geochemical Evidence for Changes in the Upper Oceanic Crust." *AGU Geophysical Monograph Volume 148*, pp. 285-304.

Wanninkhof, R., J.R. Ledwell, W.S. Broecker, M. Hamilton. (1987). "Gas exchange on Mono Lake and Crowley Lake, California", *Journal of Geophysical Research, Volume* 92, *Number C13,* pp.14,567-14,580.

Wheat C.G., M.J. Mottl. (2000). "Composition of pore and spring waters from Baby Bare: Global implications of geochemical fluxes from a ridge flank hydrothermal system." *Geochimica et Cosmochimica Acta, Volume* 64, pp. 629-642.

Wheat, C.G., H. Elderfield, M.J. Mottl, C. Monnin. (2000). "Chemical composition of basement fluids within an oceanic ridge flank: Implications for along-strike and across-strike hydrothermal circulation", *Journal of Geophysical Research, Volume 105, Number B6,* pp.13,437-13,447.

Wheat, C.G., H.W. Jannasch, M. Kastner, J.N. Plant, E.H. DeCarlo. (2003). "Seawater transport and reaction in upper oceanic basaltic basement: chemical data from continuous monitoring of sealed boreholes in a ridge flank environment." *Earth and Planetary Science Letters, Volume 216, Number 4*, pp. 549-564.

Wheat, G.C., H.W. Jannasch, A.T. Fisher, K. Becker, J. Sharkey, S. Hulme. (2010). "Subseafloor seawater-basalt-microbe reactions: Continuous sampling of borehole fluids in a ridge flank environment." *Geochemistry,Geophysics,Geosystems, Volume 11, Number 7*.

Wheat, C.G., S.M. Hulme, A.T. Fisher, B.N. Orcutt, K.Becker. (2013). "Seawater recharge into oceanic crust: IODP Exp 327 Site U1363 Grizzly Bare outcrop", *Geochemistry, Geophysics, Geosystems*, *Volume 14*, pp. 1,957-1,972.

Wilson, R.D., D.M. Mackay. (1996). "SF_6 as a Conservative Tracer in Saturated Media with High Intragranular Porosity or High Organic Carbon Content", *Ground Water, Volume 34,* pp. 241-249.

Winslow, D.M., A.T. Fisher, K. Becker. (2013). "Characterizing borehole fluid flow and formation permeability in the ocean crust using linked analytic models and Markov chain Monte Carlo analysis" *Geochemistry, Geophysics, Geosystems*, *Volume 14*, pp. 3,857-3,874.

Zindler, A., E. Jagoutz. (1988). "Mantle Cryptology", *Geochimica et Cosmochimica Acta Volume 52, Number 2,* pp. 319-333.

APPENDIX A

SITE	1301A	EXPEDITION DRILLED	IODP 301	CORK INSTALLED	2004
LATITUDE	47°45.209'N	LONGTITUDE	127°45.833'W	SEAFLOOR DEPTH	2667 m
SEDIMENT THICKNESS	262 m	BASEMENT DEPTH	108 m	CASED INTERVAL	0 m – 277 m
CORK LEAKING	YES	OS DATA GAPS	7/3/11 – 4/23/12	OS LEAKING	COIL 2

Coil number: 1		Date Deployed: 06/24/2010		Date Retrieved: 07/04/2011		
Distance Along Coil (m)	Date Analyzed	OS Sample Date	Days After Injection	Mean $[SF_6]$ (nmol/L)	±	n
202.25	10/5/2012	7/1/2010	-55.7	0.14	0.00	1
192.25	10/5/2012	7/17/2010	-39.3	0.11	0.02	3
182.25	10/5/2012	8/5/2010	-20.1	0.12	0.00	2
172.25	10/5/2012	8/23/2010	-2.7	0.11	0.03	3
162.25	10/5/2012	9/10/2010	15.6	0.10	0.02	3
152.25	10/4/2012	9/28/2010	33.9	0.27	0.05	3
142.25	10/4/2012	10/17/2010	52.2	0.10	0.03	3
132.25	10/4/2012	11/4/2010	70.4	0.33	0.06	3
122.25	10/4/2012	11/22/2010	88.7	0.12	0.06	3
112.25	9/26/2012	12/11/2010	107.0	0.11	0.03	3
102.25	9/26/2012	12/29/2010	125.3	0.14	0.09	3
92.25	9/26/2012	1/16/2011	143.6	0.22	0.20	3
82.75	9/26/2012	2/3/2011	161.9	0.14	0.04	3
72.25	9/26/2012	2/22/2011	180.1	0.15	0.05	3
62.25	9/26/2012	3/12/2011	198.4	0.08	0.07	3
52.25	9/26/2012	3/30/2011	216.7	0.23	0.13	3

42.25	9/24/2012	4/17/2011	235.0	0.15	0.03	3
32.25	9/24/2012	5/6/2011	253.3	0.11	0.02	3
27.25	8/22/2012	5/15/2011	262.4	3.99	0.18	3
13.25	8/21/2012	6/10/2011	288.0	12.42	3.51	3
2.75	8/30/2012	6/29/2011	307.2	22.16	11.35	3
Coil number: 2		Date Deployed: 07/03/2011		Date Retrieved: 07/06/2013		
Distance Along Coil (m)	Date Analyzed	OS Sample Date	Days After Injection	Mean [SF_6] (nmol/L)	±	n
273.97	8/23/2013	4/23/2012	606.3	0.03	7.06	2
261.5	8/23/2013	5/3/2012	616.5	0.01	3.10	3
251.5	8/23/2013	5/11/2012	624.7	0.01	3.63	3
241.5	8/26/2013	5/19/2012	632.1	0.01	0.00	3
231.5	8/26/2013	5/27/2012	640.3	0.00	0.00	3
221.5	8/26/2013	6/4/2012	648.9	0.00	0.50	3
211.5	8/26/2013	6/13/2012	657.5	0.00	1.25	3
201.5	8/26/2013	6/22/2012	666.1	0.00	1.10	3
191.5	8/26/2013	6/29/2012	673.9	0.00	0.00	3
181.5	8/26/2013	7/8/2012	682.1	0.00	0.00	3
171.5	8/26/2013	7/16/2012	690.3	0.00	0.58	3
161.5	8/26/2013	7/23/2012	697.7	0.00	0.00	3
151.5	8/26/2013	8/1/2012	706.7	0.00	0.61	3
141.5	8/26/2013	8/9/2012	714.9	0.00	0.00	3
131.5	8/26/2013	8/18/2012	723.1	0.00	0.00	3
121.5	8/26/2013	8/26/2012	731.3	0.00	0.00	3
111.5	8/26/2013	9/2/2012	738.7	0.00	0.00	3
101.5	8/26/2013	9/12/2012	748.5	0.02	0.00	3
91.5	8/26/2013	9/19/2012	755.9	0.00	0.00	3
81.5	8/26/2013	9/27/2012	763.7	0.00	0.11	3
71.5	8/26/2013	10/6/2012	772.7	0.01	4.08	3
61.5	8/26/2013	10/13/2012	779.6	0.00	0.00	3

51.5	8/26/2013	10/22/2012	788.7	0.00	0.00	3
41.5	8/26/2013	10/30/2012	796.9	0.00	0.00	3
31.5	8/26/2013	11/7/2012	804.7	0.00	0.67	3
21.5	8/26/2013	11/16/2012	813.3	0.00	0.00	3
11.5	8/26/2013	11/24/2012	821.5	0.00	0.00	3
1.6	8/26/2013	12/2/2012	829.8	0.00	0.00	3
Coil number: 3		Date Deployed: 07/03/2011		Date Retrieved: 07/06/2013		
Distance Along Coil (m)	Date Analyzed	OS Sample Date	Days After Injection	Mean $[SF_6]$ (nmol/L)	±	n
273.0	6/13/2014	12/3/2012	830.9	0.02	0.00	1
271.5	6/13/2014	12/6/2012	834.0	0.00	0.00	2
261.5	6/13/2014	12/15/2012	842.2	0.00	0.00	2
251.5	6/13/2014	12/23/2012	850.4	0.00	0.00	2
241.75	6/13/2014	12/31/2012	858.4	0.00	0.86	2
231.5	6/13/2014	1/8/2013	866.8	0.00	0.00	3
221.5	6/13/2014	1/16/2013	875.0	0.00	0.00	3
211.5	6/13/2014	1/25/2013	883.2	0.00	0.00	3
201.5	6/13/2014	2/2/2013	891.4	0.00	0.00	3
191.5	5/29/2014	2/10/2013	899.6	0.00	0.00	3
181.5	5/29/2014	2/18/2013	907.8	0.00	0.00	3
171.5	5/29/2014	2/26/2013	916.0	0.00	0.00	3
161.5	5/29/2014	3/7/2013	924.2	0.00	0.00	3
151.5	5/29/2014	3/15/2013	932.4	0.00	0.00	3
141.5	5/29/2014	3/23/2013	940.6	0.00	0.00	3
131.5	5/29/2014	3/31/2013	948.8	0.00	0.00	3
121.5	5/29/2014	4/8/2013	957.0	0.00	0.00	3
111.5	5/29/2014	4/17/2013	965.1	0.00	0.00	3
101.5	5/29/2014	4/25/2013	973.3	0.00	0.00	3
91.5	5/29/2014	5/3/2013	981.5	0.00	0.00	3
81.5	5/29/2014	5/11/2013	989.7	0.00	0.00	3

71.5	5/29/2014	5/19/2013	997.9	0.00	0.00	3
61.5	5/29/2014	5/28/2013	1006.1	0.00	0.00	3
51.5	5/29/2014	6/5/2013	1014.3	0.00	0.00	1
41.5	5/29/2014	6/13/2013	1022.5	0.00	0.00	3
30.5	5/29/2014	6/22/2013	1031.6	0.01	0.00	1
21.5	5/29/2014	6/29/2013	1038.9	0.01	1.12	3

SITE	1362B	**EXPEDITION DRILLED**	IODP 327	**CORK INSTALLED**	2010
LATITUDE	47°45.499'N	**LONGTITUDE**	127°45.733'W	**SEAFLOOR DEPTH**	2672 m
SEDIMENT THICKNESS	242 m	**BASEMENT DEPTH**	110 m	**CASED INTERVAL**	0 m – 312 m
CORK LEAKING	NO	**OS DATA GAPS**	7/8/11 – 8/24/11	**OS LEAKING**	COIL 1

Coil number: 1		Date Deployed: 07/08/2011		Date Retrieved: 07/14/2013		
Distance Along Coil (m)	Date Analyzed	OS Sample Date	Days After Injection	Mean [SF_6] (nmol/L)	±	n
274.8	8/28/2013	8/29/2011	368.4	3.56	0.13	2
261.5	8/28/2013	9/14/2011	384.7	3.27	0.16	2
251.5	8/28/2013	9/27/2011	397.2	3.87	0.05	2
241.5	8/28/2013	10/9/2011	409.7	3.41	0.12	2
231.5	8/28/2013	10/22/2011	422.2	3.68	0.06	2
221.5	8/28/2013	11/3/2011	434.7	3.87	0.30	2
211.5	8/28/2013	11/16/2011	447.3	3.58	0.40	2
201.5	8/28/2013	11/28/2011	459.8	3.29	0.14	2
191.5	8/28/2013	12/11/2011	472.3	3.20	0.28	2
181.5	8/28/2013	12/23/2011	484.8	2.91	0.06	2
171.5	8/28/2013	1/5/2012	497.3	3.32	0.22	2
161.5	8/27/2013	1/17/2012	509.8	2.18	0.08	2

151.5	8/27/2013	1/30/2012	522.4	2.08	0.04	2
141.5	8/27/2013	2/11/2012	534.9	2.45	0.21	2
111.5	8/27/2013	3/20/2012	572.4	2.10	0.11	2
101.5	8/27/2013	4/1/2012	584.9	2.78	1.26	1
91.5	8/27/2013	4/14/2012	597.5	1.96	0.33	2
81.5	8/27/2013	4/26/2012	610.0	2.50	0.15	2
71.5	8/27/2013	5/9/2012	622.5	2.37	0.00	2
61.5	8/27/2013	5/22/2012	635.0	2.84	0.33	2
51.5	8/27/2013	6/3/2012	647.5	2.21	0.22	2
41.5	8/27/2013	6/16/2012	660.1	36.70	3.91	2
32.0	8/27/2013	6/27/2012	671.9	27.92	24.94	2
21.5	8/27/2013	7/11/2012	685.1	1.89	0.31	2
11.5	8/27/2013	7/23/2012	697.6	2.72	0.18	2

Coil number: 2	Date Deployed: 07/08/2011	Date Retrieved: 07/14/2013

Distance Along Coil (m)	Date Analyzed	OS Sample Date	Days After Injection	Mean $[SF_6]$ (nmol/L)	±	n
261.5	1/31/2014	8/18/2012	723.1	4.49	0.35	1
251.5	1/31/2014	8/30/2012	735.6	4.80	0.35	1
241.5	1/31/2014	9/12/2012	748.2	4.90	0.51	2
231.5	1/31/2014	9/24/2012	760.7	4.97	0.24	3
221.5	1/31/2014	10/7/2012	773.2	5.05	0.35	1
211.5	1/31/2014	10/19/2012	785.7	3.86	0.35	1
201.5	1/31/2014	11/1/2012	798.2	3.55	0.04	3
191.5	1/30/2014	11/13/2012	810.7	4.07	0.35	1
181.5	1/30/2014	11/26/2012	823.3	4.13	0.35	1
171.5	1/30/2014	12/8/2012	835.8	3.55	0.20	3
161.5	1/30/2014	12/21/2012	848.3	3.45	0.35	1
151.5	1/30/2014	1/2/2013	860.8	3.28	0.14	2
141.5	1/30/2014	1/15/2013	873.3	3.22	0.35	1
131.5	1/30/2014	1/27/2013	885.9	4.19	0.19	2

121.5	1/30/2014	2/9/2013	898.4	5.66	0.35	1
111.5	1/30/2014	2/21/2013	910.9	4.11	0.35	1
101.5	1/30/2014	3/6/2013	923.4	3.16	0.35	1
91.5	1/30/2014	3/18/2013	935.9	4.13	0.35	1
81.5	1/30/2014	3/31/2013	948.4	5.53	0.38	2
71.5	1/30/2014	4/12/2013	961.0	3.17	0.35	1
61.5	1/30/2014	4/25/2013	973.5	3.39	0.35	1
51.5	1/30/2014	5/7/2013	986.0	4.01	0.35	1
31.5	1/30/2014	6/2/2013	1011.0	4.03	0.78	2
21.5	1/30/2014	6/14/2013	1023.5	4.07	0.35	1
11.5	1/30/2014	6/27/2013	1036.1	3.46	0.76	2
1.2	1/30/2014	7/9/2013	1048.6	3.64	0.23	3

SITE	1362A	**EXPEDITION DRILLED**	IODP 327	**CORK INSTALLED**	2010
LATITUDE	47°45.662'N	**LONGTITUDE**	127°45.674'W	**SEAFLOOR DEPTH**	2672 m
SEDIMENT THICKNESS	236 m	**BASEMENT DEPTH**	292 m	**CASED INTERVAL**	0 m – 471 m
CORK LEAKING	NO	**OS DATA GAPS**	7/5/11 – 11/25/11	**OS LEAKING**	COIL 1

Coil number: 1	Date Deployed: 07/05/2011	Date Retrieved: 07/16/2013

Distance Along Coil (m)	Date Analyzed	OS Sample Date	Days After Injection	Mean [SF_6] nmol/L	±	n
261.5	11/21/2013	12/6/2011	467.4	6.90	0.69	3
251.5	11/25/2013	12/17/2011	478.4	7.03	1.33	3
241.5	11/21/2013	12/28/2011	489.4	5.83	2.91	3
231.5	11/25/2013	1/8/2012	500.4	6.40	0.69	3
221.5	11/21/2013	1/19/2012	511.4	7.12	1.29	3
211.5	11/21/2013	1/30/2012	522.4	9.72	1.46	3

201.5	11/8/2013	2/10/2012	533.9	6.18	0.26	2
191.5	11/8/2013	2/21/2012	544.4	6.20	3.68	3
181.5	11/8/2013	3/3/2012	555.4	2.78	0.92	3
171.5	11/15/2013	3/14/2012	566.4	4.93	3.41	3
161.5	11/15/2013	3/25/2012	577.4	4.74	0.40	3
151.5	11/25/2013	4/5/2012	588.4	5.07	0.43	3
141.5	11/25/2013	4/16/2012	599.4	4.32	1.13	2
131.5	11/22/2013	4/27/2012	610.4	4.67	1.48	3
121.5	11/22/2013	5/8/2012	621.4	3.63	0.06	3
111.5	11/22/2013	5/19/2012	632.4	5.31	0.27	3
101.5	11/22/2013	5/30/2012	643.4	5.31	0.86	3
91.5	11/22/2013	6/10/2012	654.4	4.75	2.07	3
81.5	11/22/2013	6/21/2012	665.4	4.46	1.25	3
71.5	11/21/2013	7/2/2012	676.4	3.74	0.37	3
61.5	11/21/2013	7/13/2012	687.4	3.51	0.80	3
51.5	11/21/2013	7/24/2012	698.4	2.71	0.87	3
41.5	11/20/2013	8/4/2012	709.4	4.85	1.94	3
31.5	11/8/2013	8/15/2012	720.4	6.16	0.18	3
21.5	11/7/2013	8/25/2012	730.8	5.97	0.07	3
11.5	11/7/2013	9/6/2012	742.1	5.78	0.32	3
1.3	11/7/2013	9/17/2012	753.6	6.02	0.38	4

Coil number: 2	Date Deployed: 07/05/2011	Date Retrieved: 07/16/2013

Distance Along Coil (m)	Date Analyzed	OS Sample Date	Days After Injection	Mean $[SF_6]$ (nmol/L)	±	n
271.5	6/13/2014	9/20/2012	756.3	5.60	0.14	3
261.5	6/13/2014	10/1/2012	767.3	5.64	0.06	3
251.5	6/13/2014	10/12/2012	778.3	5.46	0.10	3
241.5	6/13/2014	10/23/2012	789.3	5.00	0.20	3
231.5	6/13/2014	11/3/2012	800.3	4.68	0.07	3
221.5	6/13/2014	11/14/2012	811.3	5.41	0.95	3

211.5	6/13/2014	11/25/2012	822.3	5.37	1.11	3
201.5	6/13/2014	12/6/2012	833.3	4.51	0.06	3
191.5	5/29/2014	12/17/2012	844.3	4.59	0.49	3
181.5	5/29/2014	12/28/2012	855.3	4.09	0.01	3
171.5	5/29/2014	1/8/2013	866.3	3.70	0.06	3
161.5	5/29/2014	1/19/2013	877.3	3.74	0.05	3
151.5	5/29/2014	1/30/2013	888.3	3.85	0.03	3
141.5	5/29/2014	2/10/2013	899.3	3.89	0.04	3
131.5	5/29/2014	2/21/2013	910.3	3.80	0.11	3
121.5	5/29/2014	3/4/2013	921.3	3.47	0.03	3
111.5	5/29/2014	3/15/2013	932.3	3.10	0.08	3
101.5	5/29/2014	3/26/2013	943.3	3.26	0.06	3
91.5	5/29/2014	4/6/2013	954.3	3.20	0.07	3
81.5	5/29/2014	4/17/2013	965.3	3.12	0.03	3
71.5	5/29/2014	4/28/2013	976.3	2.99	0.05	3
61.5	5/29/2014	5/9/2013	987.3	2.63	0.06	3
51.5	5/29/2014	5/20/2013	998.3	2.66	0.11	3
41.5	5/29/2014	5/31/2013	1009.3	2.71	0.09	3
31.5	5/29/2014	6/11/2013	1020.3	2.51	0.07	3
21.5	5/29/2014	6/22/2013	1031.3	2.38	0.03	3
11.5	5/29/2014	7/3/2013	1042.3	2.40	0.04	3
5.0	4/28/2014	7/9/2013	1048.9	2.12	0.07	9

SITE	1026B	EXPEDITION DRILLED	IODP 168/301	CORK INSTALLED	1996/2004
LATITUDE	47°45.759'N	LONGTITUDE	127°45.552'W	SEAFLOOR DEPTH	2658 m
SEDIMENT THICKNESS	229 m	BASEMENT DEPTH	48 m	CASED INTERVAL	0 m – 277 m
CORK LEAKING	YES	OS DATA GAPS	See Text	OS LEAKING	COIL 2

Coil number: 1	Date Deployed: 06/28/2010	Date Retrieved: 07/06/2011

Distance Along Coil (m)	Date Analyzed	OS Sample Date	Days After Injection	Mean [SF_6] (nmol/L)	±	n
1.6	1/21/2013	n/a	n/a	0.10	0.08	3
11.5	1/21/2013	n/a	n/a	0.07	0.04	3
21.5	1/21/2013	n/a	n/a	0.07	0.01	2
31.5	1/21/2013	n/a	n/a	0.03	0.01	3
41.5	1/21/2013	n/a	n/a	0.02	0.02	3
51.5	1/21/2013	n/a	n/a	0.02	0.01	3
61.5	1/21/2013	n/a	n/a	0.01	0.00	3
71.5	1/21/2013	n/a	n/a	0.03	0.03	3
81.5	1/21/2013	n/a	n/a	0.06	0.00	3
91.5	1/21/2013	n/a	n/a	0.01	0.00	3
101.5	1/21/2013	n/a	n/a	0.01	0.01	3
111.5	1/28/2013	n/a	n/a	0.00	0.00	3
121.5	1/28/2013	n/a	n/a	0.01	0.00	3
131.5	1/28/2013	n/a	n/a	0.00	0.00	3
141.5	1/28/2013	n/a	n/a	0.00	0.00	3
151.5	1/28/2013	n/a	n/a	0.01	0.00	3
161.5	1/28/2013	n/a	n/a	0.00	0.00	2
171.5	1/29/2013	n/a	n/a	0.00	0.00	2
181.5	1/29/2013	n/a	n/a	0.01	0.00	3
191.5	1/29/2013	n/a	n/a	0.01	0.00	2
201.5	1/29/2013	n/a	n/a	0.00	0.00	3

211.5	1/29/2013	n/a	n/a	0.00	0.00	3
221.5	1/29/2013	n/a	n/a	0.00	0.00	3
231.5	1/29/2013	n/a	n/a	0.00	0.00	3
241.5	1/29/2013	n/a	n/a	0.00	0.00	3
251.5	1/29/2013	n/a	n/a	0.01	0.00	3
261.5	1/29/2013	n/a	n/a	0.01	0.00	3

Coil: Injectate	Injection Start: 8/26/2010	Injection End: 8/27/2010	
Distance Along Coil (m)	Date Analyzed	Mean $[SF_6]$ (µmol/L)	n
15.45	2/23/2012	83.89	1
15.70	2/23/2012	58.89	1
16.00	2/23/2012	1.45	1
16.37	2/23/2012	2.36	1
16.37	2/23/2012	2.52	1
16.62	2/23/2012	100.74	1
16.62	2/23/2012	100.30	1
16.87	2/23/2012	71.63	1
16.87	2/23/2012	69.33	1
16.87	2/23/2012	72.36	1
16.87	2/23/2012	71.43	1
17.12	2/23/2012	49.49	1
17.12	2/23/2012	51.03	1
18.37	2/23/2012	5.98	1
18.62	2/23/2012	33.44	1
18.87	2/23/2012	27.58	1
19.12	2/23/2012	33.48	1
20.37	2/23/2012	39.46	1

Coil: Injectate	Injection Start: 8/26/2010	Injection End: 8/27/2010	
Distance Along Coil (m)	Date Analyzed	Mean $[SF_6]$ (µmol/L)	n
20.62	2/23/2012	45.68	1
20.87	2/23/2012	29.92	1
21.12	2/23/2012	39.21	1
22.37	2/23/2012	42.44	1
23.12	2/23/2012	32.85	1
24.87	2/23/2012	1.01	1
26.62	2/23/2012	1.30	1
26.87	2/23/2012	0.59	1
28.37	2/23/2012	1.22	1
29.12	2/23/2012	2.57	1
30.32	2/23/2012	0.39	1
31.12	2/23/2012	2.04	1
31.50	8/22/2013	2.26	1
32.25	8/22/2013	1.57	1
33.00	8/22/2013	0.15	1
33.75	8/22/2013	0.78	1
34.50	8/22/2013	0.62	1
35.25	8/22/2013	0.09	1
36.00	8/22/2013	0.01	1
36.75	8/22/2013	0.01	1
37.50	8/22/2013	0.01	1
38.25	8/22/2013	0.01	1
39.00	8/22/2013	n/d	1
39.75	8/22/2013	n/d	1
40.50	8/22/2013	0.00	1
41.25	8/22/2013	0.00	1
42.00	8/22/2013	0.00	1

Coil: Injectate	Injection Start: 8/26/2010	Injection End: 8/27/2010	
Distance Along Coil (m)	Date Analyzed	Mean $[SF_6]$ (µmol/L)	n
42.75	8/22/2013	0.00	1
43.50	8/22/2013	0.00	1
44.25	8/22/2013	0.00	1
45.00	8/22/2013	0.00	1
45.75	8/22/2013	0.00	1
46.50	8/22/2013	0.00	1
47.25	8/22/2013	0.00	1
48.00	8/22/2013	0.00	1
48.75	8/22/2013	0.00	1
49.50	8/22/2013	0.00	1
50.25	8/22/2013	n/a	1
51.25	8/22/2013	n/d	1
52.25	8/22/2013	0.00	1
53.25	8/22/2013	0.00	1
54.25	8/22/2013	n/d	1
55.25	8/22/2013	n/d	1
56.25	8/22/2013	0.00	1
57.25	8/22/2013	0.00	1
58.25	8/22/2013	0.00	1
59.25	8/22/2013	0.00	1
60.25	8/22/2013	0.00	1
61.25	8/22/2013	0.00	1
62.25	8/22/2013	0.00	1
63.25	8/22/2013	0.00	1
64.25	8/22/2013	0.00	1
65.25	8/22/2013	0.00	1
66.25	8/22/2013	0.00	1

Coil: Injectate	Injection Start: 8/26/2010	Injection End: 8/27/2010	
Distance Along Coil (m)	Date Analyzed	Mean [SF_6] (µmol/L)	n
67.25	8/22/2013	0.00	1
68.25	8/22/2013	n/d	1
69.25	8/22/2013	0.00	1
70.25	8/22/2013	0.00	1
71.25	8/22/2013	0.00	1
72.25	8/22/2013	0.00	1
73.25	8/22/2013	0.00	1
74.25	8/22/2013	0.00	1
75.25	8/22/2013	0.00	1
76.25	8/22/2013	0.00	1

---

n = number of samples analyzed where concentrations and distances were averaged (if n>1)
date analyzed = based on seawater-freshwater interface given by Moss Landing Research Center
date deployed = exact time *ROV Jason* entered ocean as OS pumps began pumping
date retrieved = time *ROV Jason* landed on deck